Supplementary Information

Evidence for Stepwise Oxetane Formation in an $FeCl_3$ Catalyzed Carbonyl-Olefin Metathesis Reaction

Tamal Das,† Anuradha Dagar,† Chetan Joshi, Madison A. Neukirch, Mathew J. Vetticatt* and Jennifer S. Hirschi*

Department of Chemistry, Binghamton University, Binghamton, New York 13902, United States.

*Email: jhirschi@binghamton.edu vetticatt@binghamton.edu † These authors contributed equally.

Table of Contents

Supplementary Note 1. General experimental methods 1

Supplementary Note 2. General procedure for the synthesis of (E)-1-(2'-styryl-[1,1'-biphenyl]-2-yl) ethanone: 2

Supplementary Note 3. Procedure for ^{13}C KIE experiments 3

Supplementary Note 4. Conformational sampling of selected geometries before applying DFT methods. 13

Supplementary Note 5. Details of Computational Methods 14

Supplementary Note 6. Ab initio molecular dynamics simulations 19

Supplementary Note 7. Ab initio Metadynamics study 20

Supplementary Note 8. Free Energy Surface Calculations with ab initio Metadynamics 20

Supplementary Note 9. Canonical Variational Transition State (CVT) calculation 23

Supplementary Note 10. AIMD downhill quasi-classical direct dynamics 27

Supplementary Note 11. Comments on ^{13}C KIE interpretation Schindler and Kwan ChemRxiv 2022 29

Supplementary Note 12. Free energy surfaces calculated using various DFT methods 32

Supplementary Note 13. Progdyn.conf file 38

Supplementary Note 14. CP2K metadynamics input file 42

Supplementary Note 15. Gaussrate sample Input File: 45

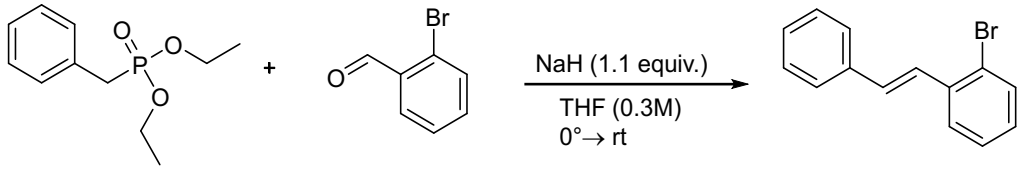
Supplementary References 54

Supplementary Note 1. General experimental methods

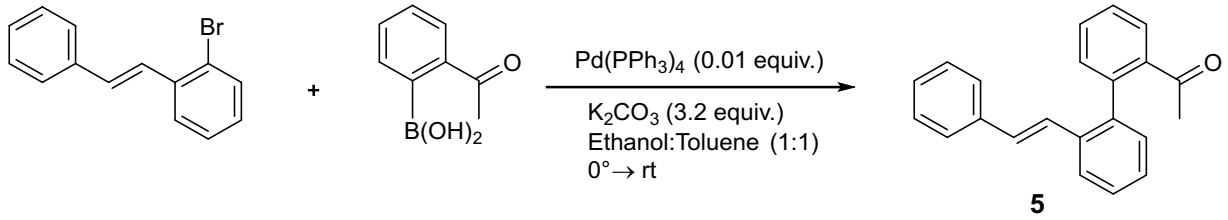
Unless specified, all reagents and starting materials were purchased from commercial sources and used as received. "Concentrated" refers to the removal of volatile solvents via distillation using a

rotary evaporator. “Dried” refers to pouring onto, or passing through, anhydrous magnesium sulfate followed by filtration. Flash chromatography was performed using silica gel (230−400 mesh) with hexanes and ethyl acetate as the eluents. All reactions were monitored by Nuclear Magnetic Resonance Spectroscopy (NMR). ^{1}H, and ^{13}C NMR spectra were recorded on a 600 MHz Bruker NMR spectrometer or 400 MHz Bruker NMR in $CDCl_3$ and were described as chemical shifts in ppm, multiplicity (s, singlet; d, doublet; t, triplet; q, quartet; doublet−doublet (dd), pentet (p), m, multiplet), coupling constant in hertz (Hz), and number of protons.

Supplementary Note 2. General procedure for the synthesis of (E)-1-(2'-styryl-[1,1'-biphenyl]-2-yl) ethanone:



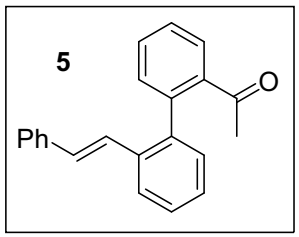
The starting material precursor (E)-1-bromo-2-styrylbenzene was synthesized according to the procedure of Schindler et al.[1] To a 250 ml round-bottom flask equipped with a Teflon septum and magnetic stir bar were added diethyl benzyl phosphonate (22.0 mmol, 1.1 equiv.) and dry THF (0.3M, 60 mL). The solution was cooled to 0°C in an ice bath and NaH (24.0 mmol, 1.2 equiv.) was added to the solution. After stirring at 0°C for 30 minutes, 2-bromobenzaldehyde (20.0 mmol, 1.0 equiv.) was slowly added. The reaction was stirred at room temperature for 12h. The reaction progress was monitored by NMR and quenched by aqueous ammonium chloride at 0°C. The solution was extracted with ethyl acetate, dried over $MgSO_4$, and concentrated to afford (E)-1-bromo-2-styrylbenzene for direct use in the next step.



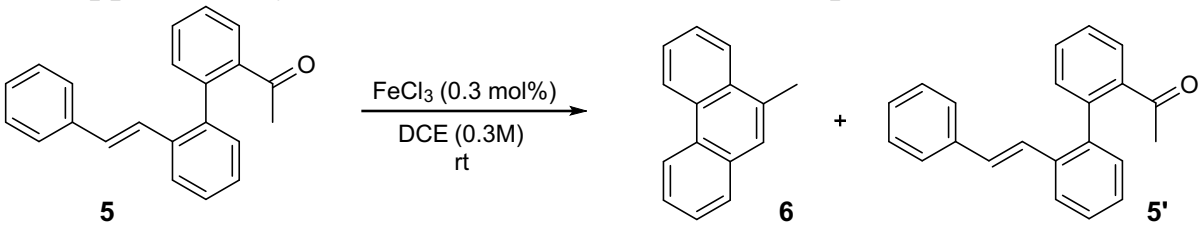
To a 250 mL round-bottom flask equipped with a magnetic stir bar and condenser were added K_2CO_3 (64.0 mmol, 3.2 equiv.), Tetrakis(triphenylphosphine)palladium(0) (1.28 mmol, 2.0 mol %) and 2-acetylphenylboronic acid (24.0 mmol, 1.2equiv.). The flask was sealed and purged under nitrogen for 10 minutes. (E)-1-Bromo-2-styrylbenzene (20.0 mmol, 1.0 eq) dissolved in a solution of toluene/ethanol (1:1, 0.2M, 100ml) was added to the flask and the solution was refluxed at 80°C

for 8h. The reaction progress was monitored by NMR, and once complete, the solution was allowed to cool to room temperature. The mixture was concentrated to remove toluene/ethanol and then extracted with ethyl acetate and water, dried over $MgSO_4$, and purified by silica gel column chromatography (EtOAc:hexane, 3:97) to afford a mixture of (E)-1-(2'-styryl-[1,1'-biphenyl]-2-yl)ethanone and (Z)-1-(2'-styryl-[1,1'-biphenyl]-2-yl)ethanone (96.4:3.6), which upon crystallization gives E-isomer (**5**).

(E)-1-(2'-Styryl-[1,1'-biphenyl]-2-yl) ethanone. Compound **5** was synthesized according to general procedure to give a white solid. **^{1}H NMR (400 MHz, $CDCl_3$)** δ_H 7.79 (d, *J* = 7.8 Hz, 1H), 7.73 (d, *J* = 7.6 Hz, 1H), 7.55 (td, *J* = 7.4, 1.4 Hz, 1H), 7.41 – 7.50 (m, 2H), 7.28 – 7.36 (m, 6H), 7.21 – 7.30 (m, 2H), 7.05 (d, *J* = 16.2 Hz, 1H), 6.91 (d, *J* = 16.2 Hz, 1H), 2.02 (s, 3H); **^{13}C{^{1}H}NMR (101 MHz, $CDCl_3$)** δ_C 202.7, 140.8, 139.9, 139.6, 137.2, 135.6, 131.5, 130.8, 130.4, 130.3, 128.6, 128.3, 128.2, 127.7, 127.6, 127.5, 126.6, 126.4, 125.5, 29.7.



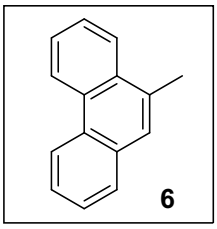
Supplementary Note 3. Procedure for ^{13}C KIE experiments



To a 250 mL round bottomed flask equipped with a Teflon septum and magnetic stir bar was added $FeCl_3$ (0.0315 mmol, 0.3 mol %) and the vial was sealed and purged under nitrogen for 10 minutes. Then, (E)-1-(2'-styryl-[1,1'-biphenyl]-2-yl)ethanone (10.5 mmol, 1.0 equiv.) in dry DCE (0.1M, 100 mL) was added to the reaction flask. The reaction mixture was stirred at room temperature. The reaction progress was monitored by NMR. After starting material conversions of 72.0% (KIE 1), 69.5% (KIE 2) and 73.3% (KIE 3) were achieved, the crude reaction mixture is filtered through a sintered disc packed with silica and eluted with dichloromethane until all product was eluted (determined by TLC) and concentrated under reduced pressure. The reaction products and unreacted starting material were isolated using silica gel column chromatography (hexane = 100%) to afford unreacted (E)-1-(2'-styryl-[1,1'-biphenyl]-2-yl)ethanone (**5**). The ^{13}C isotopic

compositions of each KIE sample (KIE 1, KIE 2, KIE 3) were compared to a respective independent unreacted standard sample (STD 1, STD 2, STD 3).

9-Methylphenanthrene. Compound **6** was isolated from the experiment used to measure KIEs (procedure described above) as a white crystalline solid. **^{1}H NMR (400 MHz, $CDCl_3$)** δ_H 8.77 (d, *J* = 9.4 Hz, 1H), 8.70 (d, *J* = 8.8 Hz, 1H), 8.10 (d, *J* = 9.4 Hz, 1H), 7.85 (d, *J* = 9.1 Hz, 1H), 7.66 – 7.70 (m, 2H), 7.60 – 7.64 (m, 3H), 2.78 (s, 3H); **^{13}C{^{1}H}NMR (100 MHz, $CDCl_3$)** δ_C 132.5, 132.1, 132.0, 130.4, 129.7, 127.8, 126.7, 126.6, 126.5, 126.2, 125.8, 124.7, 123.0, 122.5, 20.0.



Sample Preparation for ^{13}C KIE analysis

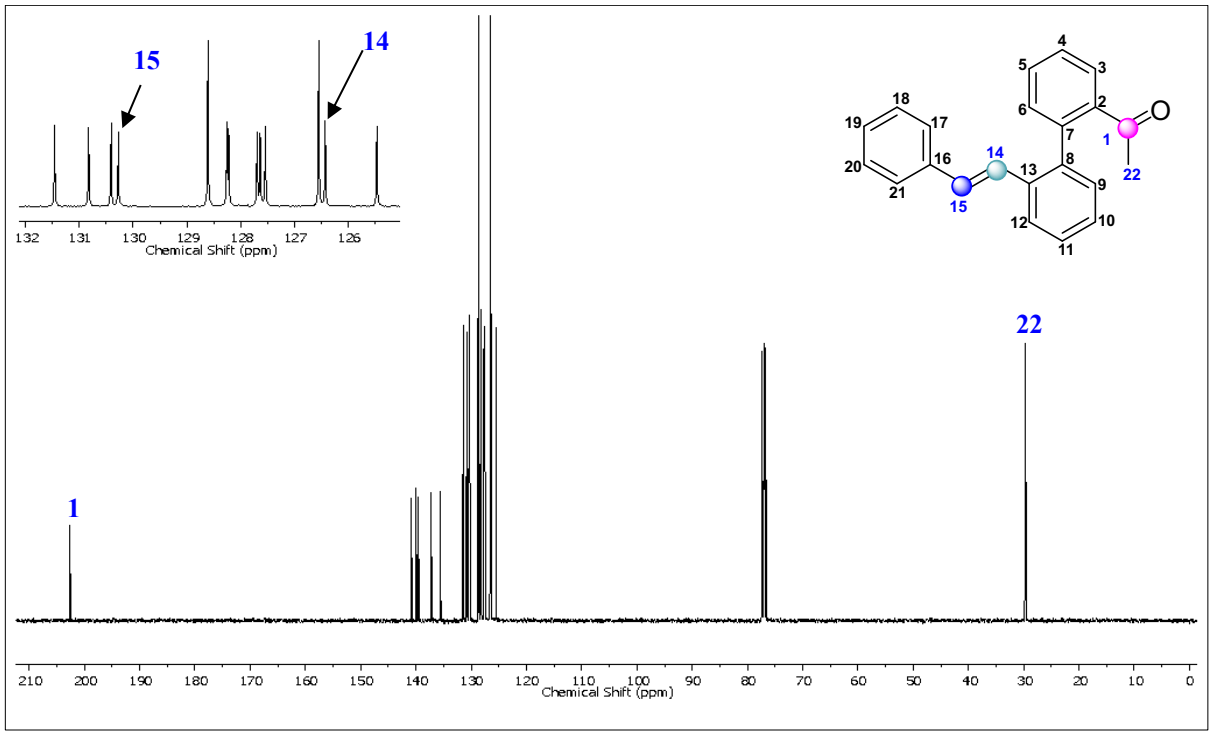
For each KIE experiment, six independent measurements were conducted using specified parameters on a 600 MHz Bruker NMR spectrometer for both KIE and standard (STD) samples (3 sets of KIE experiments). The acquisition time for each sample was determined based on the spectral peak width and the number of points collected for the spectrum to ensure the digital resolution of each peak was sufficient for quantitative ^{13}C NMR analysis. For each pair of samples (eg. KIE1/STD1), integrations for each peak were numerically determined using a constant integration range equal to 10 times the average peak-widths at half-height for that peak. Isotope effects were calculated for each pair of measurements, averaged, and a 95% confidence range (C) was calculated from the 18 individual isotope effects.

$$C = \frac{t_{p,v}\, S}{\sqrt{n}}$$

where **S** is the standard deviation, n is the number of measurements, and $t_{p,v}$ is distribution function corresponding to confidence level n-1. This methodology was applied uniformly to all KIE measurements performed in this study.

1. (E)-1-(2'-styryl-[1,1'-biphenyl]-2-yl)ethanone NMR analysis- Supplementary Fig. 1

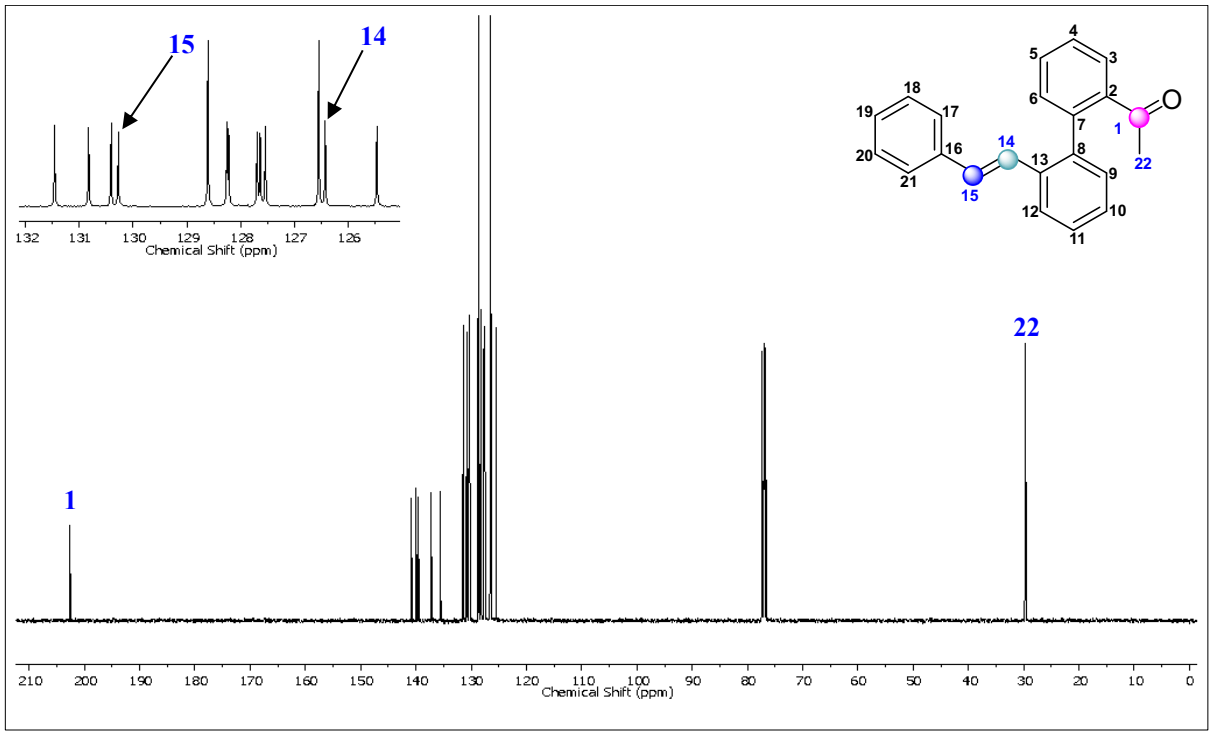
NMR parameters for KIE determination
KIE1/STD1
Acquisition time = 5 sec
Delay time = 17.5 s (7 times T1 relaxation time (2.5) of slowest relaxing peak)
Number of transients = 512



Supplementary Figure 1: ^{13}C NMR spectrum of (E)-1-(2'-styryl-[1,1'-biphenyl]-2-yl)ethanone in $FeCl_3$ catalyzed RCCOM obtained for determination of ^{13}C KIEs (run 1).

2. (E)-1-(2'-styryl-[1,1'-biphenyl]-2-yl)ethanone NMR analysis- Supplementary Fig. 2

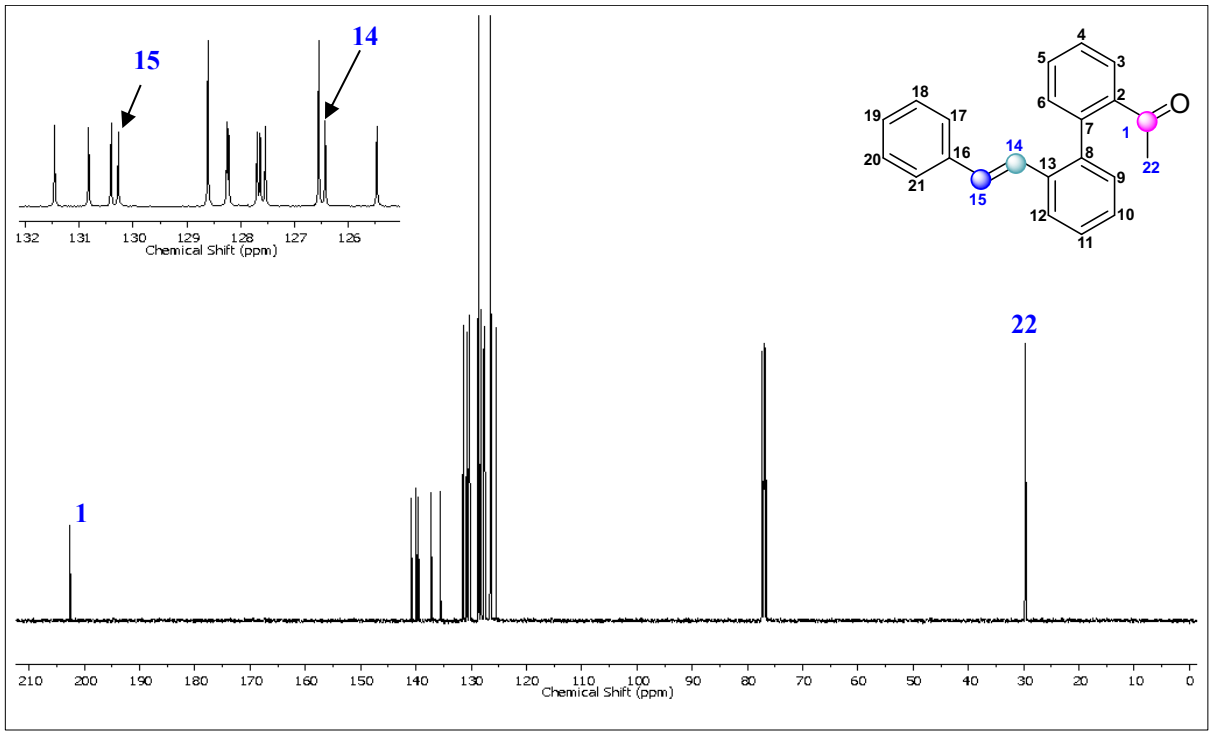
NMR parameters for KIE determination
KIE2/STD2
Acquisition time = 5 sec
Delay time = 17.5 s (7 times T1 relaxation time (2.5) of slowest relaxing peak)
Number of transients = 512



Supplementary Figure 2: ^{13}C NMR spectrum of (E)-1-(2'-styryl-[1,1'-biphenyl]-2-yl)ethanone in $FeCl_3$ catalyzed RCCOM obtained for determination of ^{13}C KIEs (run 2).

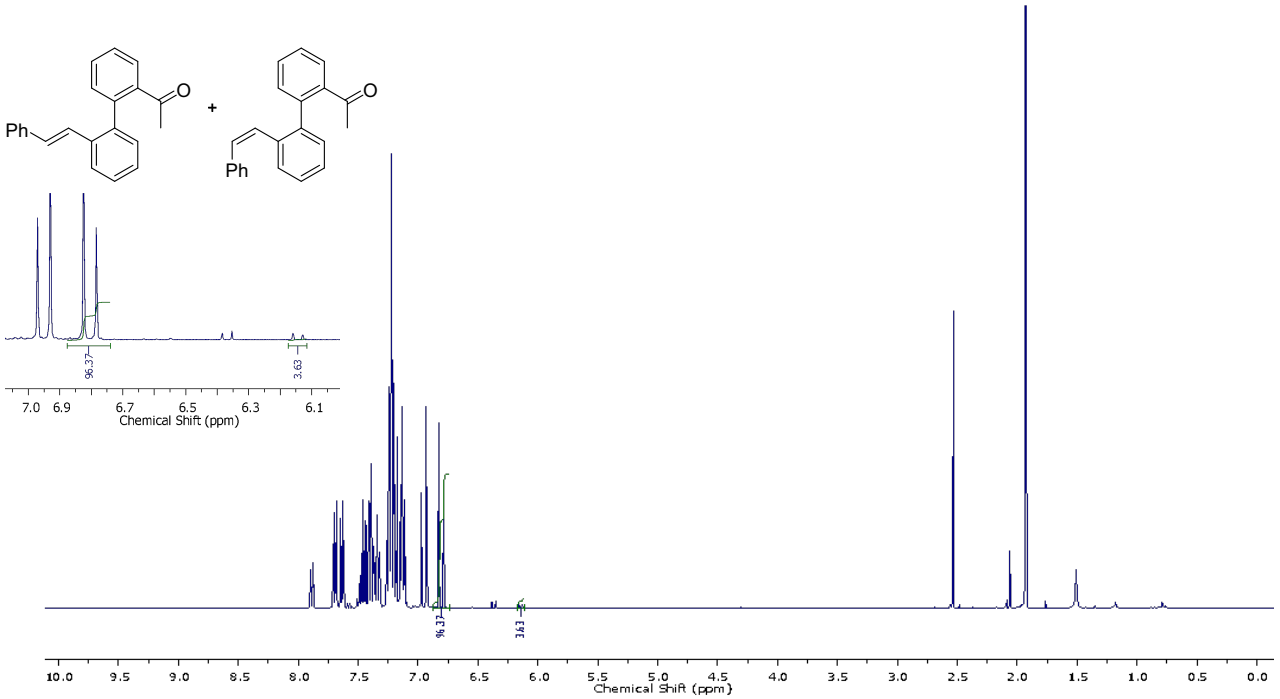
3. (E)-1-(2'-styryl-[1,1'-biphenyl]-2-yl)ethanone NMR analysis - Supplementary Fig. 3

NMR parameters for KIE determination
KIE1/STD1
Acquisition time = 5 sec
Delay time = 17.5 s (7 times T1 relaxation time (2.5) of slowest relaxing peak)
Number of transients = 512

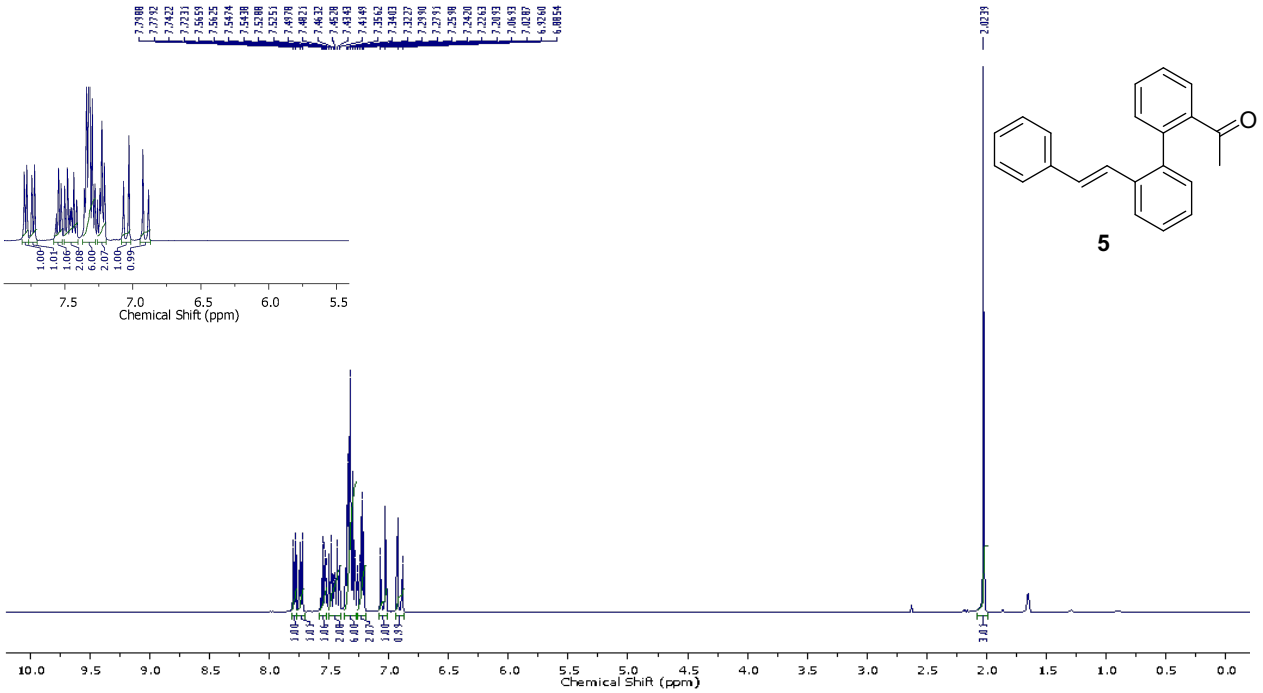


Supplementary Figure 3: ^{13}C NMR spectrum of (E)-1-(2'-styryl-[1,1'-biphenyl]-2-yl)ethanone in $FeCl_3$ catalyzed RCCOM obtained for determination of ^{13}C KIEs (run 3).

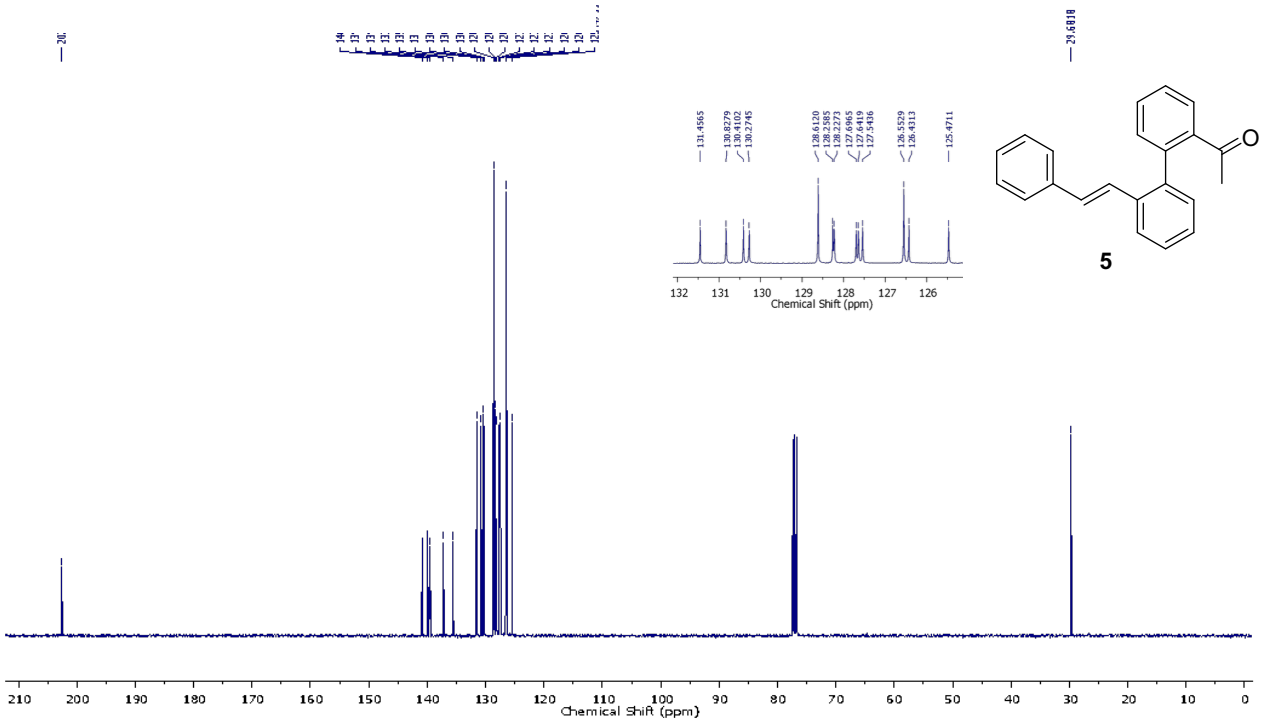
^{1}H NMR spectra of the mixture of E and Z isomers



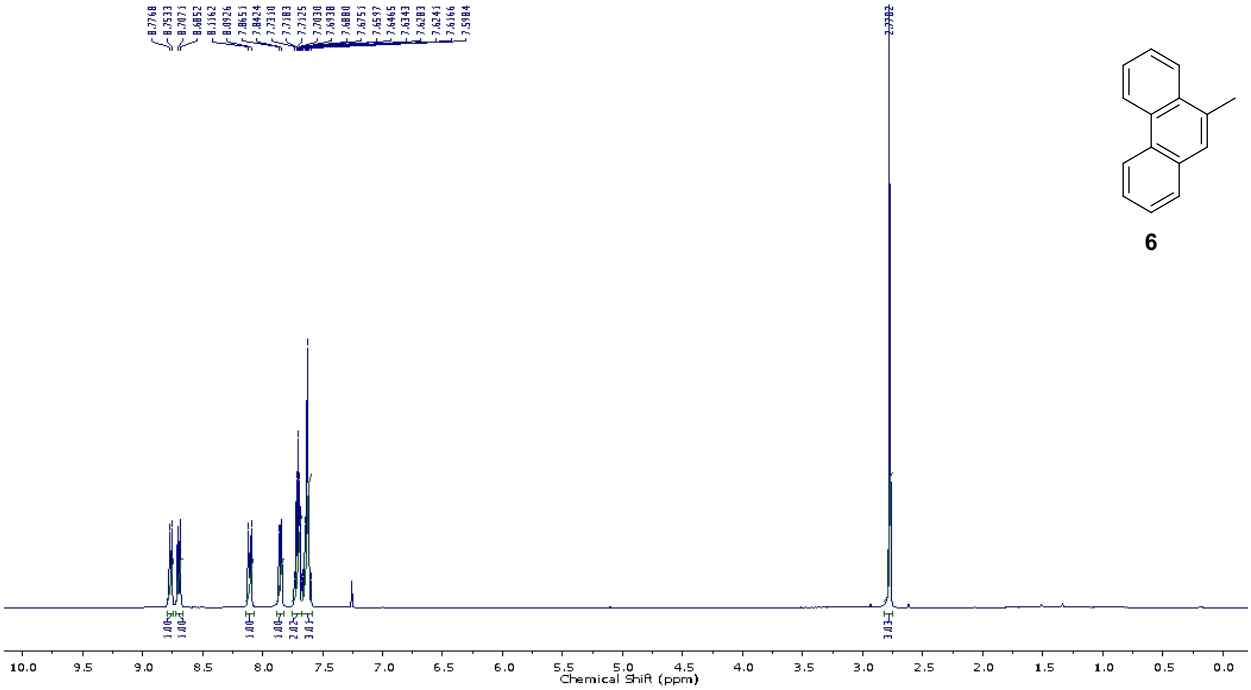
^{1}H NMR spectra of E isomer



^{13}C NMR spectra of E isomer

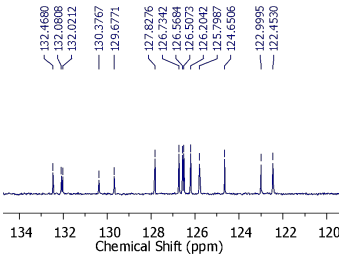


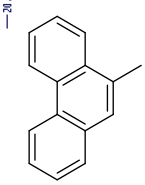
^{1}H NMR spectra of the product



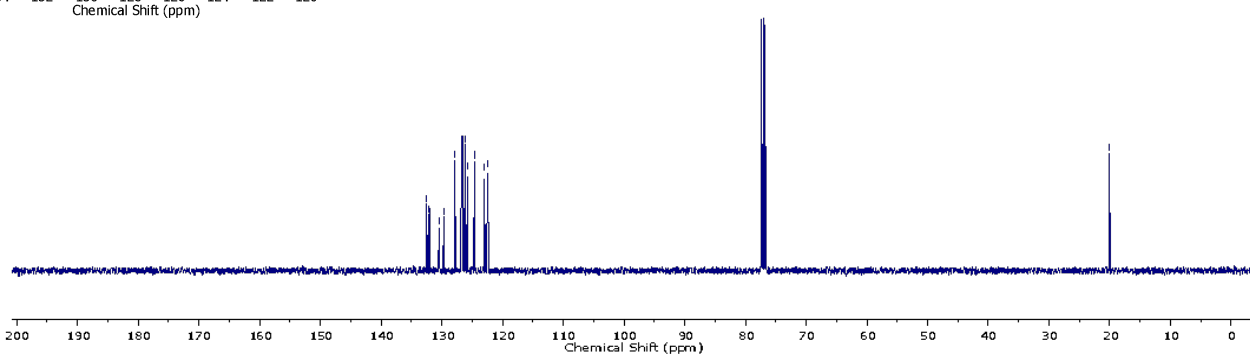
6

^{13}C NMR spectra of the Product

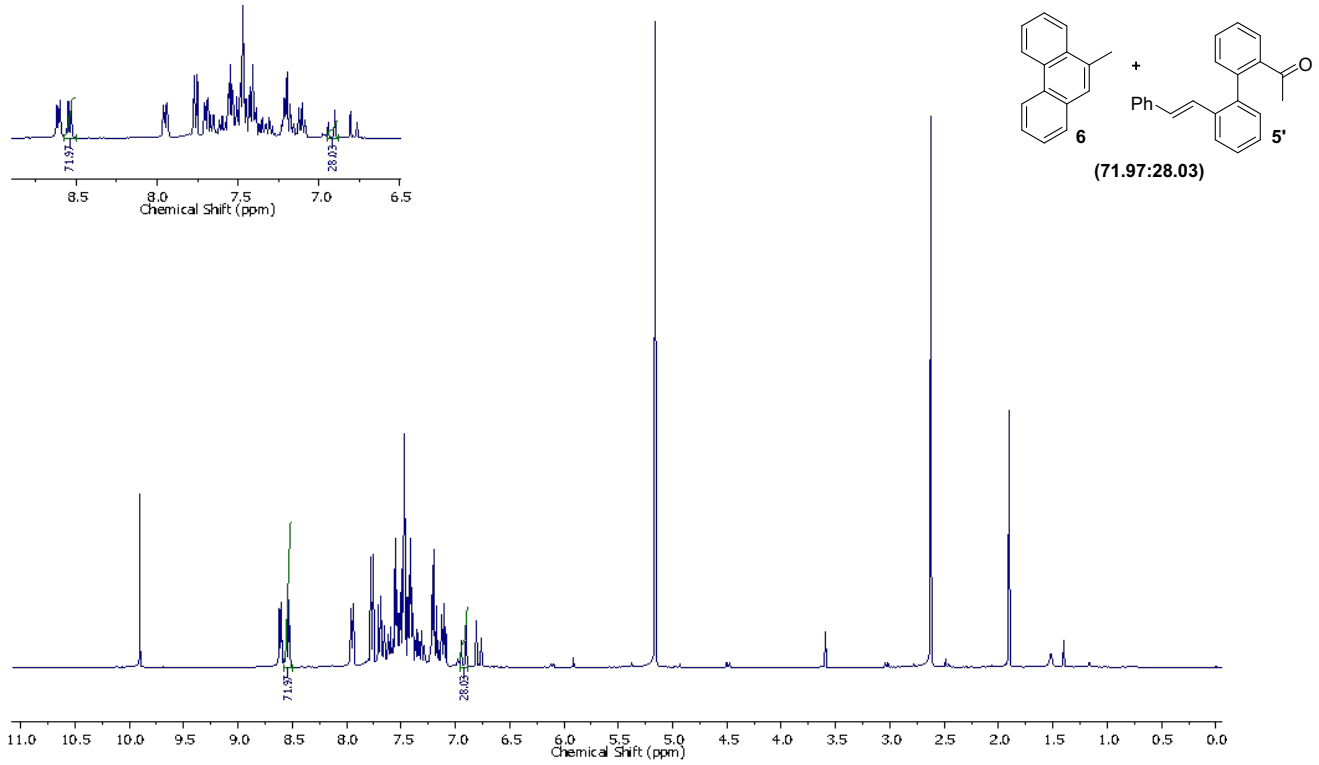




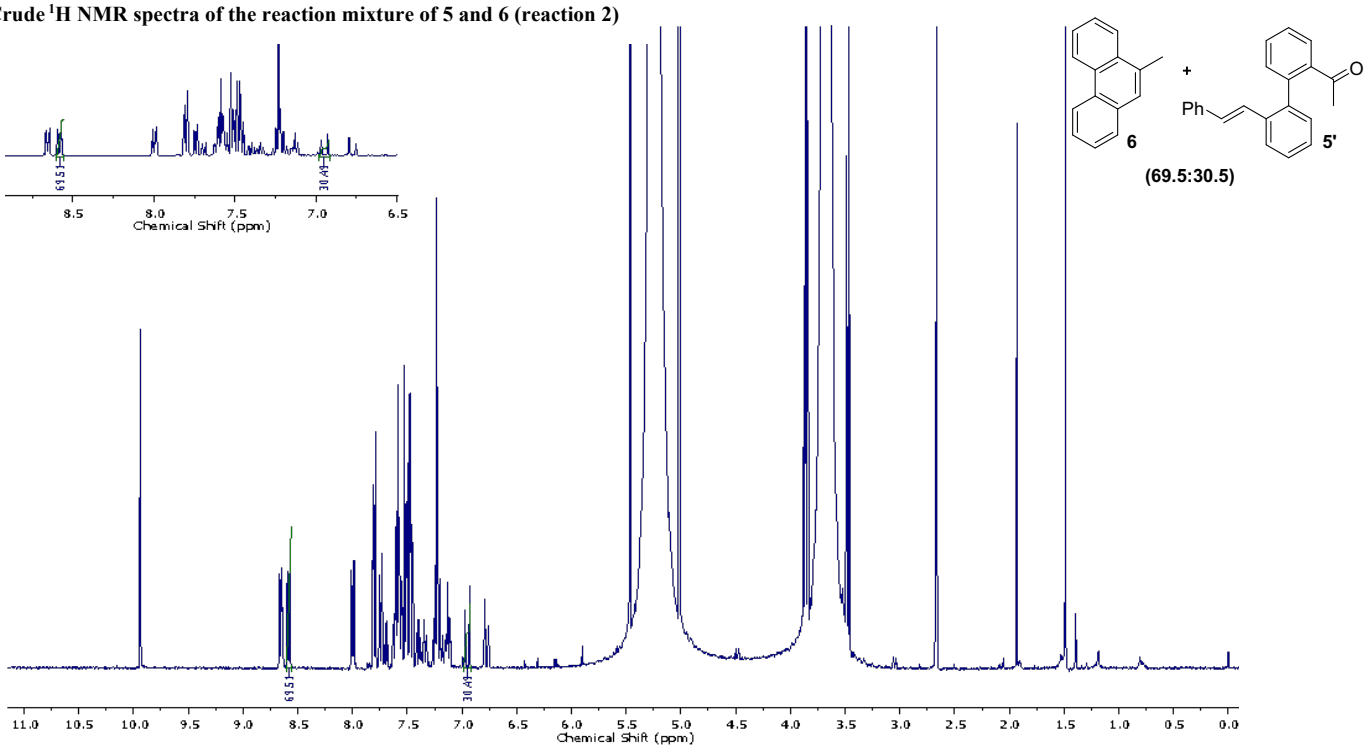
6



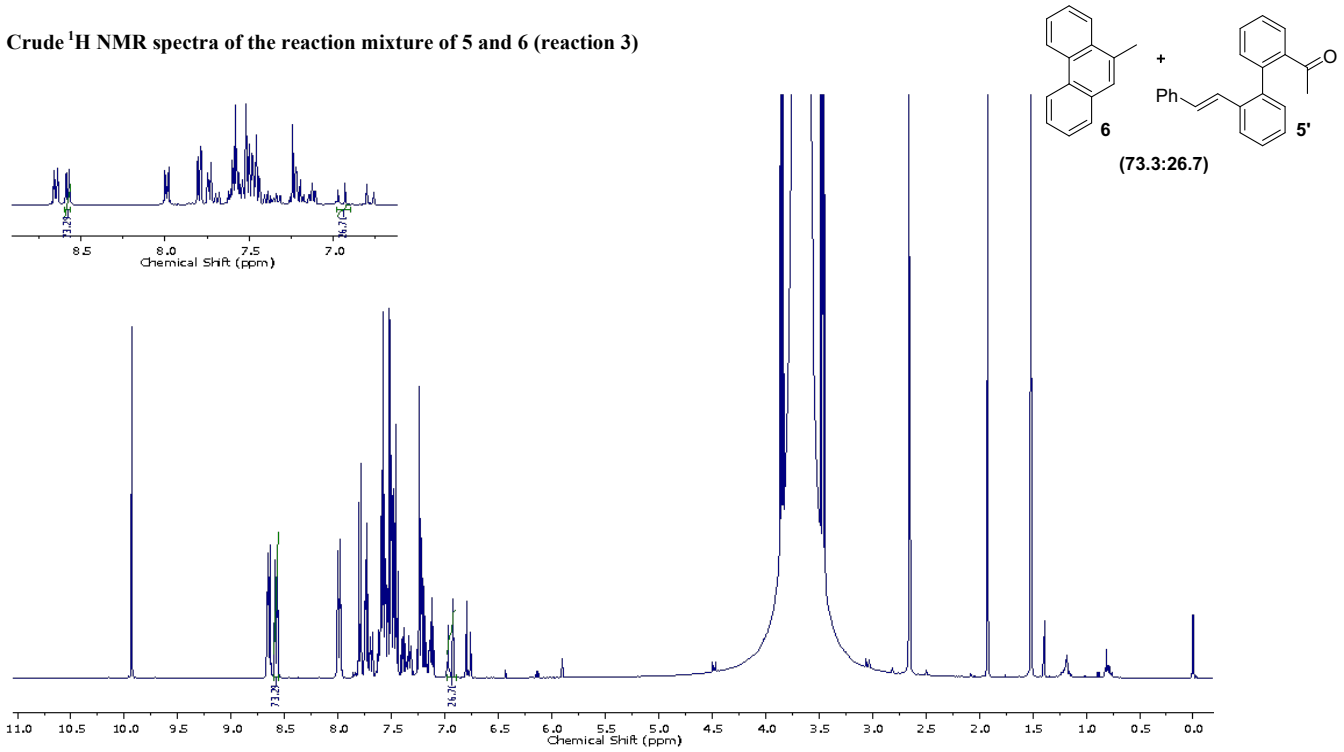
Crude ^{1}H NMR spectra of the reaction mixture of 5 and 6 (reaction 1)



Crude ^{1}H NMR spectra of the reaction mixture of 5 and 6 (reaction 2)



Crude ^{1}H NMR spectra of the reaction mixture of 5 and 6 (reaction 3)



(E)-1-(2'-styryl-[1,1'-biphenyl]-2-yl)ethanone from reaction − NMR analysis-Supplementary Table 1

NMR parameters for KIE determination

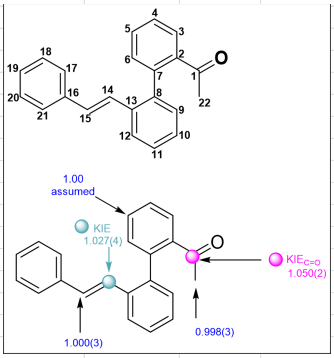
KIE1/STD1

Acquisition time = 5 sec

Delay time = 17.5 s (7 times T1 relaxation time (2.5) of slowest relaxing peak)

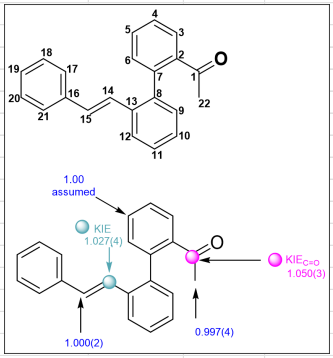
Number of transients = 512

Standard -1								
peak	**fid1**	**fid2**	**fid3**	**fid4**	**fid5**	**fid6**	**average**	**stddev**
1	1028.9000	1028.2000	1028.7000	1024.9000	1026.3000	1028.7000	1027.6167	1.6400
2	1005.1000	1007.9000	1007.4000	1005.0000	1006.2000	1008.7000	1006.7167	1.5250
3	1008.7000	1012.8000	1013.2000	1012.0000	1011.8000	1013.3000	1011.9667	1.7143
4	998.6000	1000.2000	1001.2000	1000.4000	1001.8000	1003.0000	1000.8667	1.5055
5	1020.7000	1022.2000	1021.3000	1024.3000	1024.1000	1024.9000	1022.9167	1.7486
6	1024.4000	1027.8000	1029.5000	1026.2000	1028.3000	1028.0000	1027.3667	1.7985
7	1000.0000	1000.0000	1000.0000	1000.0000	1000.0000	1000.0000	1000.0000	0.0000
8	1007.8000	1005.9000	1007.8000	1008.3000	1006.5000	1012.6000	1008.1500	2.3603
9	1019.3000	1023.1000	1021.3000	1022.3000	1018.3000	1022.3000	1021.1000	1.8974
10	1012.0000	1012.5000	1014.6000	1014.4000	1014.4000	1012.8000	1013.4500	1.1450
11	2009.9000	2013.4000	2012.9000	2014.2000	2012.3000	2014.8000	2012.9167	1.7268
12	2020.8000	2021.5000	2024.4000	2025.2000	2020.7000	2025.7000	2023.0500	2.3002
13	1034.2000	1036.3000	1034.9000	1038.5000	1039.6000	1038.7000	1037.0333	2.2196
14	998.1000	1003.2000	1003.8000	1002.3000	1004.0000	1004.8000	1002.7000	2.4033
15	1062.9000	1066.7000	1067.8000	1067.7000	1067.6000	1070.2000	1067.1500	2.3873



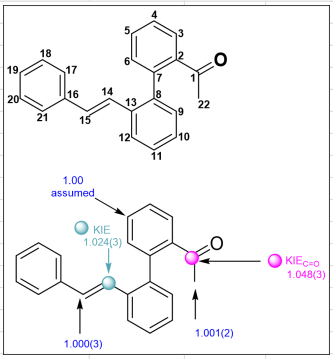
Experimental KIE - 1									%Conv:	0.72
peak	**fid1**	**fid2**	**fid3**	**fid4**	**fid5**	**fid6**	**average**	**stddev**	**KIE**	**stdev**
1	1092.6000	1092.8000	1092.6000	1093.2000	1091.1000	1089.2000	1091.9167	1.5105	**1.050**	0.002
2	1000.3000	1002.6000	1004.5000	1002.3000	998.4000	999.0000	1001.1833	2.3473	**0.996**	0.003
3	1011.8000	1012.1000	1011.0000	1014.6000	1009.9000	1007.8000	1011.2000	2.2812	**0.999**	0.003
4	1002.9000	1006.3000	1004.7000	1004.1000	999.6000	999.3000	1002.8167	2.8301	**1.002**	0.003
5	1020.2000	1021.9000	1024.3000	1023.4000	1018.9000	1020.4000	1021.5167	2.0624	**0.999**	0.003
6	1027.1000	1028.3000	1029.4000	1028.8000	1024.6000	1023.2000	1026.9000	2.4835	**1.000**	0.003
7	1000.0000	1000.0000	1000.0000	1000.0000	1000.0000	1000.0000	1000.0000	0.0000	**1.000**	0.000
8	1007.3000	1008.3000	1010.1000	1008.9000	1004.6000	1010.5000	1008.2833	2.1507	**1.000**	0.003
9	1021.4000	1023.7000	1022.7000	1024.3000	1020.5000	1017.5000	1021.6833	2.4871	**1.000**	0.003
10	1016.7000	1016.9000	1014.4000	1015.0000	1011.5000	1014.7000	1014.8667	1.9541	**1.001**	0.002
11	2010.5000	2017.5000	2013.2000	2013.8000	2010.0000	2010.9000	2012.6500	2.8233	**1.000**	0.002
12	2004.1000	2008.9000	2007.8000	2007.5000	2001.4000	2002.9000	2005.4333	3.0448	**0.993**	0.002
13	1070.6000	1074.6000	1076.0000	1071.4000	1066.5000	1071.6000	1071.7833	3.3229	**1.027**	0.004
14	1005.6000	1004.4000	1005.0000	1001.6000	1003.1000	1000.9000	1003.4333	1.8960	**1.001**	0.003
15	1064.1000	1066.4000	1067.5000	1067.1000	1063.7000	1060.9000	1064.9500	2.5265	**0.998**	0.003

Standard - 2								
peak	**fid1**	**fid2**	**fid3**	**fid4**	**fid5**	**fid6**	**average**	**stddev**
1	1029.249	1029.6890	1034.2610	1029.1180	1034.2490	1029.2630	1030.9715	2.5506
2	1008.0456	1011.0780	1012.0950	1010.2200	1008.5720	1006.4420	1009.4088	2.0986
3	1000.5840	1006.3340	1009.9350	1008.6630	1005.7520	1003.9880	1005.8760	3.3478
4	994.8900	1000.0870	1003.3090	1000.4520	999.0990	995.7240	998.9268	3.1451
5	1019.3920	1020.5400	1024.4940	1020.7090	1022.5940	1017.2450	1020.8290	2.5122
6	1024.3290	1024.8920	1030.9600	1027.9560	1030.3300	1026.1570	1027.4373	2.7866
7	1000.0000	1000.0000	1000.0000	1000.0000	1000.0000	1000.0000	1000.0000	0.0000
8	1006.2340	1007.1310	1010.8890	1007.9860	1008.0540	1006.2000	1007.7490	1.7370
9	1021.3670	1023.2230	1024.9570	1023.9550	1023.8280	1019.6660	1022.8327	1.9540
10	1012.6580	1012.8090	1015.0530	1013.1290	1015.8340	1010.1003	1013.2639	2.0202
11	2005.7930	2011.4420	2019.9720	2011.7870	2014.3080	2009.4710	2012.1288	4.7762
12	2003.3710	2007.5970	2016.2540	2008.5900	2008.2130	2006.0380	2008.3438	4.3186
13	1040.9950	1045.9090	1048.6040	1042.8180	1046.5260	1041.5296	1044.3969	3.0596
14	1002.1380	1001.7370	1003.1170	1000.6080	1001.0240	1003.1230	1001.9578	1.0466
15	1066.0450	1067.2120	1075.9300	1070.2680	1072.0360	1069.0390	1070.0883	3.5686



Experimental KIE - 2									%Conv:	0.695
peak	**fid1**	**fid2**	**fid3**	**fid4**	**fid5**	**fid6**	**average**	**stddev**	**KIE**	**stdev**
1	1091.3040	1090.0650	1089.8180	1092.3500	1092.9910	1089.4750	1091.0005	1.4475	**1.050**	0.003
2	1003.1540	1003.7410	1005.3890	1006.0820	1007.6670	1003.3720	1004.9008	1.7899	**0.996**	0.003
3	1006.1510	1005.3180	1007.7360	1005.3150	1008.8500	1007.4290	1006.7998	1.4351	**1.001**	0.004
4	996.8640	998.7570	997.0010	998.7310	1003.4840	997.3880	998.7042	2.4847	**1.000**	0.004
5	1018.2070	1017.9410	1019.5520	1020.0780	1021.1010	1018.0450	1019.1540	1.2962	**0.999**	0.003
6	1025.0430	1025.4590	1024.5260	1025.7350	1029.3190	1021.3930	1025.2458	2.5408	**0.998**	0.004
7	1000.0000	1000.0000	1000.0000	1000.0000	1000.0000	1000.0000	1000.0000	0.0000	**1.000**	0.000
8	1007.3910	1009.1390	1008.3190	1007.6470	1011.0060	1007.3550	1008.4762	1.4132	**1.001**	0.002
9	1022.4200	1022.4410	1021.5180	1023.2160	1024.9170	1021.8510	1022.7272	1.2199	**1.000**	0.002
10	1016.8170	1012.6070	1009.9250	1012.5570	1016.7550	1010.4430	1013.1840	2.9937	**1.000**	0.004
11	2014.0560	2015.0850	2014.3880	2013.0660	2019.3900	2006.8470	2013.8053	4.0545	**1.001**	0.003
12	2006.4350	2006.5810	2006.0940	2004.2190	2012.6390	2002.6640	2006.4387	3.3988	**0.999**	0.003
13	1077.3790	1076.4900	1078.2360	1078.1180	1081.8710	1073.1790	1077.5455	2.8186	**1.027**	0.004
14	998.3990	1002.1680	998.5080	1000.4090	1004.2200	999.8790	1000.5972	2.2512	**0.999**	0.002
15	1066.2630	1066.4870	1066.5840	1067.0890	1068.8700	1065.2160	1066.7515	1.2080	**0.997**	0.004

Standard - 3								
peak	**fid1**	**fid2**	**fid3**	**fid4**	**fid5**	**fid6**	**average**	**stddev**
1	1025.7000	1023.0000	1021.5000	1028.1000	1024.9000	1027.8000	1025.1667	2.6090
2	1011.4000	1007.2000	1006.2000	1010.7000	1008.0000	1008.9000	1008.7333	2.0156
3	1012.5000	1008.7000	1008.3000	1010.2000	1011.7000	1010.8000	1010.3667	1.6488
4	1004.8000	1004.3000	1001.8000	1008.3000	1006.3000	1007.3000	1005.4667	2.3381
5	1021.1000	1020.3000	1018.8000	1020.7000	1020.4000	1022.6000	1020.6500	1.2341
6	1025.7000	1022.1000	1023.5000	1025.5000	1023.3000	1027.3000	1024.5667	1.9211
7	1000.0000	1000.0000	1000.0000	1000.0000	1000.0000	1000.0000	1000.0000	0.0000
8	1009.1000	1004.5000	1005.3000	1007.1000	1007.2000	1010.0000	1007.2000	2.1147
9	1023.2000	1018.4000	1017.8000	1024.1000	1019.4000	1021.5000	1020.7333	2.6013
10	1016.1000	1013.2000	1016.4000	1020.8000	1015.7000	1021.1000	1017.2167	3.1070
11	2009.8000	2005.2000	2002.8000	2009.6000	2006.6000	2010.6000	2007.4333	3.0813
12	2005.2000	2000.0000	1999.0000	2008.0000	2001.8000	2005.8000	2003.3000	3.5660
13	1040.8000	1035.3000	1039.6000	1042.4000	1040.3000	1042.9000	1040.2167	2.7154
14	995.8000	996.2000	999.9000	1001.0000	997.2000	1003.7000	998.9667	3.1053
15	1065.6000	1064.7000	1061.3000	1064.5000	1066.9000	1067.3000	1065.0500	2.1575



Experimental - KIE 3									%Conv:	0.733
peak	**fid1**	**fid2**	**fid3**	**fid4**	**fid5**	**fid6**	**average**	**stddev**	**KIE**	**stdev**
1	1087.0000	1089.1000	1090.5000	1089.9000	1085.8000	1089.2000	1088.5833	1.8060	**1.048**	0.003
2	1004.9000	1007.6000	1009.6000	1011.6000	1006.7000	1008.4000	1008.1333	2.3252	**1.000**	0.003
3	1012.8000	1014.8000	1014.8000	1015.8000	1013.3000	1013.8000	1014.2167	1.1143	**1.003**	0.002
4	1007.5000	1006.5000	1010.7000	1012.2000	1006.2000	1011.1000	1009.0333	2.6028	**1.003**	0.003
5	1021.0000	1025.7000	1023.9000	1024.8000	1021.2000	1020.5000	1022.8500	2.2224	**1.002**	0.002
6	1023.4000	1027.2000	1027.4000	1028.7000	1023.7000	1026.2000	1026.1000	2.1317	**1.001**	0.003
7	1000.0000	1000.0000	1000.0000	1000.0000	1000.0000	1000.0000	1000.0000	0.0000	**1.000**	0.000
8	1009.4000	1009.1000	1009.5000	1013.5000	1009.5000	1007.0000	1009.6667	2.1097	**1.002**	0.003
9	1019.9000	1021.0000	1024.5000	1023.5000	1019.1000	1019.1000	1021.1833	2.3121	**1.000**	0.003
10	1018.6000	1015.7000	1017.2000	1021.2000	1014.2000	1018.3000	1017.5333	2.4394	**1.000**	0.004
11	2013.1000	2012.3000	2017.2000	2019.6000	2008.6000	2012.7000	2013.9167	3.9015	**1.002**	0.002
12	2003.1000	2003.6000	2006.8000	2008.8000	2001.3000	2002.8000	2004.4000	2.8150	**1.000**	0.002
13	1073.4000	1072.3000	1069.6000	1074.7000	1071.7000	1073.8000	1072.5833	1.8104	**1.024**	0.003
14	1000.5000	998.2000	999.6000	1004.6000	1000.7000	999.7000	1000.5500	2.1714	**1.001**	0.004
15	1065.1000	1066.1000	1068.4000	1068.2000	1066.2000	1067.6000	1066.9333	1.3261	**1.001**	0.002

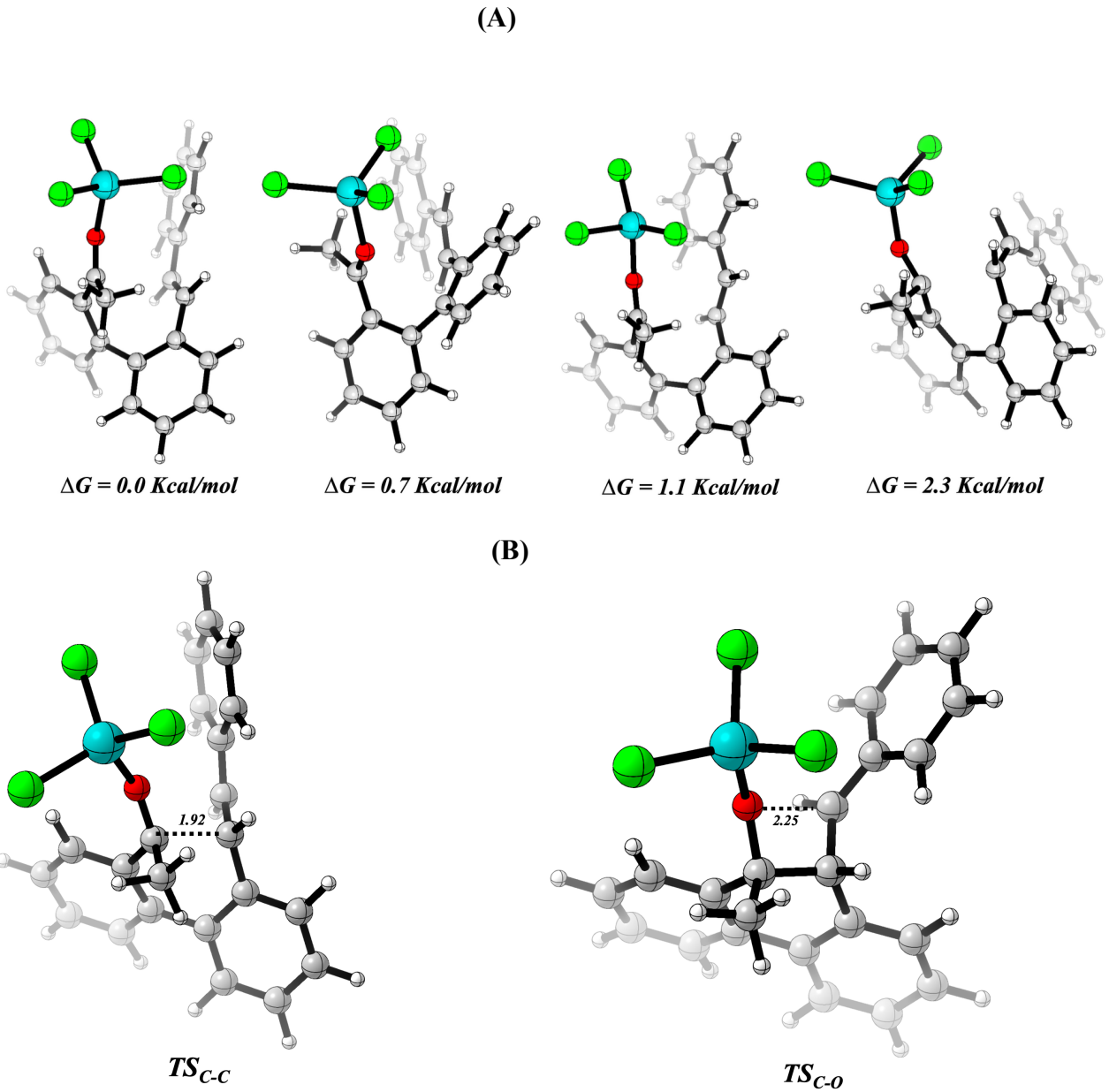
	Conver	72.0%					Conver	69.5%					Conver	73.30%							
peak	**KIE1**						**KIE2**						**KIE3**						**KIE (average)**	**stdev**	**conf**
1	1.050	1.050	1.050	1.053	1.051	1.047	1.052	1.050	1.046	1.053	1.049	1.050	1.046	1.050	1.052	1.046	1.046	1.046	**1.050**	0.002	0.001
2	0.996	0.996	0.998	0.998	0.994	0.992	0.996	0.994	0.994	0.997	0.999	0.997	0.995	1.000	1.003	1.001	0.999	1.000	**0.996**	0.002	0.001
3	1.002	0.999	0.998	1.002	0.999	0.996	1.005	0.999	0.998	0.997	1.003	1.003	1.000	1.005	1.005	1.004	1.001	1.002	**1.000**	0.003	0.001
4	1.003	1.005	1.003	1.003	0.998	0.997	1.002	0.999	0.995	0.999	1.004	1.001	1.002	1.002	1.007	1.003	1.000	1.003	**1.001**	0.003	0.001
5	1.000	1.000	1.002	0.999	0.996	0.997	0.999	0.998	0.996	0.999	0.999	1.001	1.000	1.004	1.004	1.003	1.001	0.998	**0.999**	0.002	0.001
6	1.002	1.000	1.000	1.002	0.997	0.996	1.001	1.000	0.995	0.998	0.999	0.996	0.998	1.004	1.003	1.002	1.000	0.999	**0.999**	0.002	0.001
7	1.000	1.000	1.000	1.000	1.000	1.000	1.000	1.000	1.000	1.000	1.000	1.000	1.000	1.000	1.000	1.000	1.000	1.000	**1.000**	0.000	0.000
8	1.000	1.002	1.002	1.000	0.999	0.998	1.001	1.002	0.998	1.000	1.002	1.001	1.000	1.003	1.003	1.005	1.002	0.998	**1.000**	0.002	0.000
9	1.002	1.000	1.001	1.002	1.002	0.996	1.001	0.999	0.997	0.999	1.001	1.002	0.998	1.002	1.005	1.000	1.000	0.998	**1.000**	0.002	0.001
10	1.004	1.003	1.000	1.000	0.998	1.001	1.003	1.000	0.996	1.000	1.001	1.000	1.002	1.002	1.001	1.000	0.999	0.998	**1.001**	0.002	0.001
11	1.000	1.002	1.000	1.000	0.999	0.998	1.003	1.002	0.998	1.001	1.002	0.999	1.001	1.003	1.005	1.004	1.001	1.001	**1.000**	0.002	0.000
12	0.994	0.995	0.994	0.993	0.993	0.991	1.001	1.000	0.996	0.998	1.002	0.999	0.999	1.001	1.003	1.000	1.000	0.999	**0.996**	0.004	0.001
13	1.028	1.029	1.032	1.025	1.021	1.025	1.030	1.025	1.024	1.029	1.029	1.026	1.024	1.027	1.022	1.024	1.023	1.023	**1.027**	0.003	0.001
14	1.006	1.001	1.001	0.999	0.999	0.997	0.997	1.000	0.996	1.000	1.003	0.997	1.004	1.002	1.000	1.003	1.003	0.997	**1.000**	0.003	0.001
15	1.001	1.000	1.000	1.000	0.997	0.993	1.000	0.999	0.993	0.998	0.998	0.997	1.000	1.001	1.005	1.003	1.000	1.000	**0.998**	0.003	0.001

Supplementary Table 1. NMR integrations and determination of ^{13}C KIEs for 5 (Reaction of 5 in the presence of 0.3 mol% $FeCl_3$).

Supplementary Note 4. Conformational sampling of selected geometries before applying DFT methods.

Conformational sampling was performed for the initial reactant complex (5-$FeCl_3$) to get the most stable conformation using CREST (Conformer and Rotamer Ensemble Sampling Tool), developed by Grimme and coworkers.[2] Below are a sampling of conformers of the 5-$FeCl_3$ complex with optimization and free energy calculations using the B3LYP-D3(BJ)/6-31+G* CPCM(DCE) level of theory in **Supplementary Fig. 4(A)**. Based on the calculated energies, we have taken the lowest energy conformation for calculating the potential energy surface for the COM reaction. Transition state structures (TSs) calculated from the lowest energy conformer computed at B3LYP-D3(BJ)/6-31+G* CPCM(DCE)

level of theory for the Lewis acid-catalyzed COM reaction are shown in **Supplementary Fig. 4(B).**



Supplementary Figure 4: (A) Different conformations of the 5-$FeCl_3$ complex with relative free energies. (B) Lowest energy transition state geometries ($TS_{C\text{-}C}$ and $TS_{C\text{-}O}$) located at the potential energy surface using B3LYP-D3(BJ)/6-31+G* CPCM(DCE) level of theory

Supplementary Note 5. Details of Computational Methods

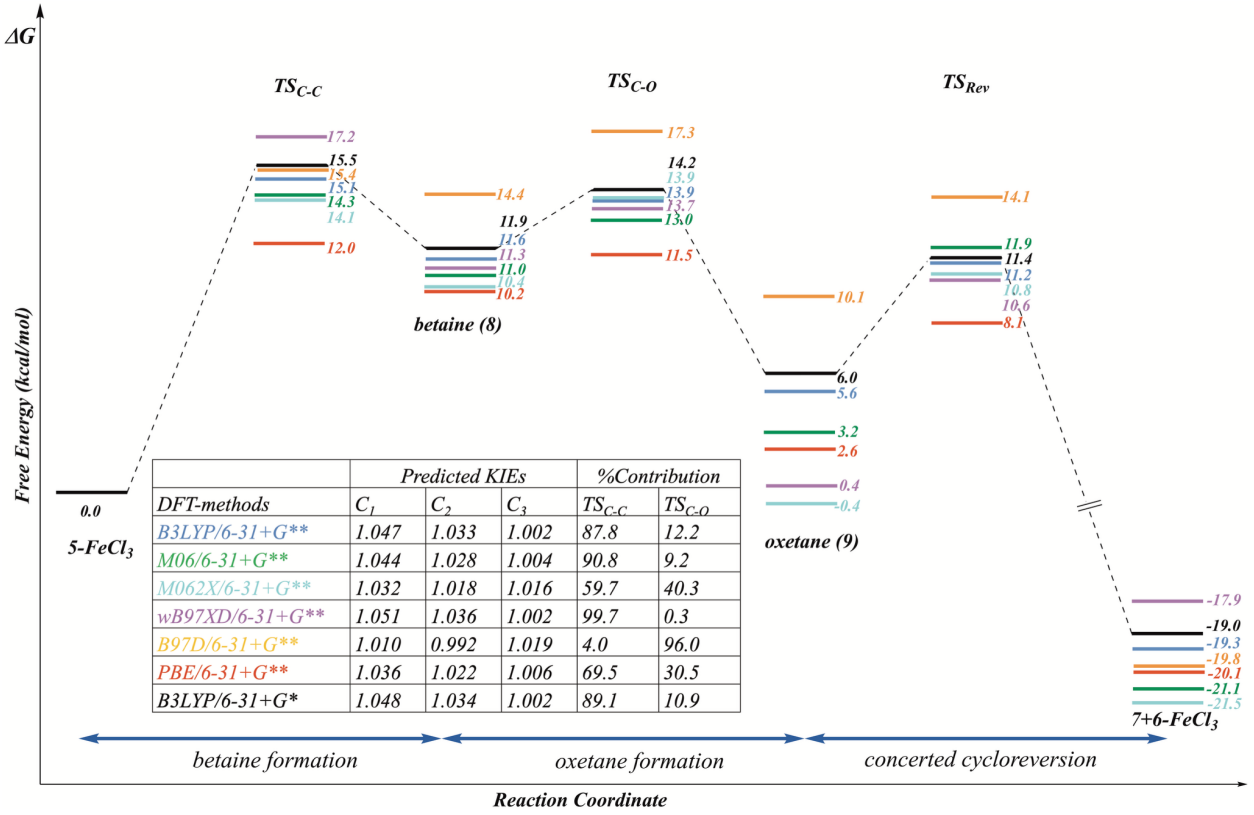
All density functional theory (DFT) calculations presented in the manuscript were primarily performed using B3LYP-D3(BJ)[3]/6-31+G*[4] CPCM,[5] (solvent = dichloroethane), level of theory

as implemented in *Gaussian 16*.[6] Ground state geometry optimizations and transition structures (TSs) were located at the B3LYP-D3(BJ)/6-31+G* level of theory, and a CPCM solvent model for dichloroethane was utilized to determine the potential energy surface shown in **Fig. 5A in the main text**. All starting materials and intermediates were verified as true minima, whereas all the transition structures were characterized by one imaginary frequency. All transition structures and intermediates for the title reaction were also computed with various sets of GGA, hybrid, and meta-GGA density functionals with Pople basis sets, e.g., PBE-D3(BJ)[7]/6-31+G** CPCM, B3LYP-D3(BJ)/6-31+G** CPCM, M06/6-31+G** CPCM, ωB97X-D/6-31+G**CPCM, B97D-D3(BJ)/6-31+G** CPCM, M06-2X/6-31+G**CPCM (solvent = dichloroethane). From the scaled vibrational frequencies of the computed transition structures, ^{13}C KIE predictions were obtained using the program PyQuiver developed by Kwan and coworkers,[8–10] and a Wigner tunneling correction was applied to the predicted values. The predicted KIEs (Fig. 5 in the main text) with all the above-mentioned levels of theory were standardized against the carbon atom assumed to be the "standard" carbon for the experimental measurements. The potential energy surface with the tabulated predicted KIEs is calculated by weighting the difference in harmonic free energies between $TS_{C\text{-}C}$ and $TS_{C\text{-}O}$ at the reaction temperature. The weighted KIEs for C1, C2, and C3 for seven methods are shown in **Supplementary Fig. 5** (these KIEs are similar to Table 1 in the main text; however, the energies are depicted on the PES in **Supplementary Fig. 5**). Further, the energy refinement was performed by single-point energy calculations and utilized to weight the KIEs for C1, C2, and C3 for the C-C and C-O bond-forming steps using the B3LYP-D3(BJ) functional, a triple-ζ Pople basis set 6-311++G**, and a CPCM solvent model for dichloroethane (ε = 10.36). Gibbs free energies were estimated at the reaction temperature of 298.15 K and were corrected using Grimme's quasi-rigid rotor harmonic oscillator approximation. Intermediates along the reaction coordinate were located by performing a quick reaction coordinate analysis (QRC) as well as an intrinsic reaction coordinate (IRC) from the respective transition structures, followed by a geometry optimization to confirm TSs and local minima of all structures in the relevant pathways (Fig. 5 in the main text).

Further, B3LYP-D3(BJ)/6-31+G* CPCM was chosen for analysis of the Singleton downhill quasiclassical dynamics to analyze the probability of recrossing events (more details in Supplementary Note 10). Additionally, the PBE-D3/DZVP-GTH CPCM method was employed in AIMD simulations using the metadynamics approach to enhance sampling of the conformational

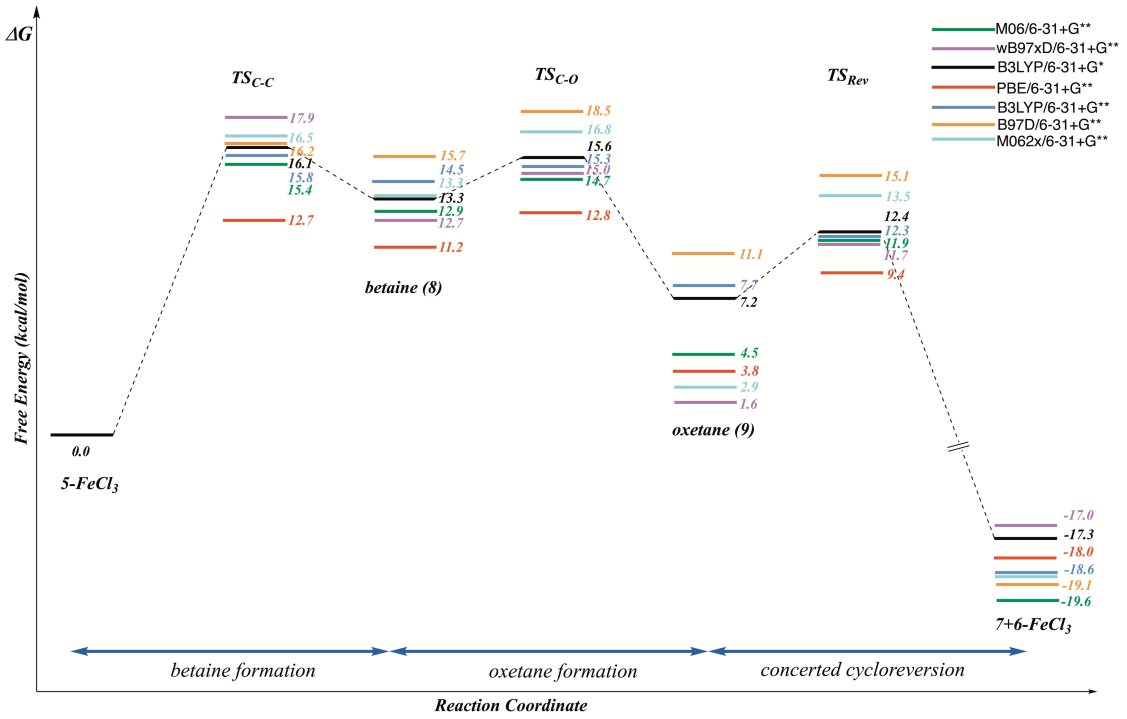
space and rare events, thereby understanding the reaction mechanism and obtaining the free energy profile for oxetane formation (more details in Supplementary Note 8). We chose these methods to avoid the high computational cost without compromising the level of theory.

The calculated energies of all computed starting materials, intermediates, and transition structures are included in Supplementary Note 12. The energy refinement using single-point correction has been implemented for all the above-mentioned levels of theories e.g. PBE-D3(BJ)/6-311++G** CPCM//PBE-D3(BJ)/6-31+G** CPCM, B97D-D3(BJ)/6-311++G** CPCM//B97D-D3(BJ)/6-31+G** CPCM, M06-2X/6-311++G** CPCM//M06-2X/6-31+G**CPCM, M06/6-311+G** CPCM//M06/6-31+G** CPCM and ωB97X-D/6-311++G**CPCM//ωB97X-D/6-31+G**CPCM (solvent = dichloroethane). The potential energy surface with the relative free energy at the reaction temperature is shown in **Supplementary Fig. 6**.



	Predicted KIEs			%Contribution	
DFT-methods	C_1	C_2	C_3	$TS_{C\text{-}C}$	$TS_{C\text{-}O}$
B3LYP/6-31+G**	1.047	1.033	1.002	87.8	12.2
M06/6-31+G**	1.044	1.028	1.004	90.8	9.2
M062X/6-31+G**	1.032	1.018	1.016	59.7	40.3
wB97XD/6-31+G**	1.051	1.036	1.002	99.7	0.3
B97D/6-31+G**	1.010	0.992	1.019	4.0	96.0
PBE/6-31+G**	1.036	1.022	1.006	69.5	30.5
B3LYP/6-31+G*	1.048	1.034	1.002	89.1	10.9

Supplementary Figure 5: Computed free energy diagram for $FeCl_3$ catalyzed COM reaction at the various DFT levels of theory (**F**/6-31+G** CPCM) indicated by the color scheme, also predicted KIE at 25 °C weighted by the difference in harmonic free energies tabulated. (**F** = B3LYP-D3(BJ), M06, M06-2X, PBE-D3(BJ), B97D, ωB97X-D). See Supplementary Table 9.



Supplementary Figure 6: Computed free energy diagram for $FeCl_3$ catalyzed COM reaction at the various DFT levels of theory with the single point energy corrections, (**F**/6-311++G** CPCM//F/6-31+G** CPCM indicated by the color scheme. (**F** = B3LYP-D3(BJ), M06, M06-2X, PBE-D3(BJ), B97D, ωB97X-D). See Supplementary Table 9.

The DFT calculation using the above mentioned levels of theory predict that the energy surface is extremely shallow over the region of **TS$_{C-C}$**, **8**, and **TS$_{C-O}$**, varying by only 1.5-3.0 kcal/mol in free energy depending upon the use of DFT method as shown in **Supplementary Fig. 5** and **Supplementary Fig. 6** (energy refinement using single-point corrections), except for ωB97X-D where the FES is deep by ~5.0 kcal/mol.

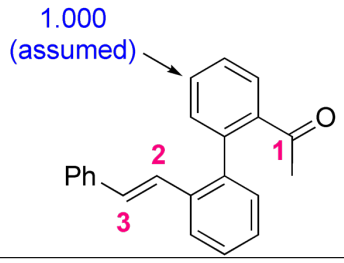
From the above-mentioned various DFT levels of theory, if we investigated the PES using B3LYP-D3(BJ)/6-31+G* (**Supplementary Fig. 5**) level of theory, the harmonic energy-weighted KIE overestimates the experimentally measured values at the C2 carbon.

^{13}C predicted KIEs with various computational methods

TS$_{C-C}$ was modeled using sixteen distinct DFT methods, including six different functionals (B3LYP-D3(BJ), M06, M06-2X, PBE, B97-D, and ωB97X-D), each with Pople (6-31+G**) basis sets as well as Karlsruhe basis set (*def2-SVP*)[11] on all atoms, including iron, as implemented in

Gaussian 16. The geometry at the transition structure is relatively independent of the method utilized; the extent of the carbon-carbon bond forming distance for $\mathbf{TS_{C\text{-}C}}$ is very similar (±0.08Å) in all the DFT methods utilized. From the scaled vibrational frequencies of the computed transition structures, ^{13}C KIE predictions were obtained using the program PyQuiver, and a Wigner tunneling correction was applied to the predicted values. The predicted KIEs reported in the manuscript (Fig. 5 in the main text) and supporting information (Supplementary Table 2) were standardized against the carbon atom assumed to be the "standard" carbon for the experimental measurements (by dividing each predicted KIE for the respective transition structure by the predicted KIE for the "standard" carbon atom).

Supplementary Table 2: ^{13}C predicted KIEs, C-C bond-distances (Å), and the imaginary vibrational mode for the key carbon-carbon bond-forming step ($\mathbf{TS_{C\text{-}C}}$) employing various computational methods (varying the functional and basis set).



Carbon#	C-1	C-2	C-3
Experimental KIEs	1.050(2) 1.050(3) 1.048(3)	1.027(4) 1.027(4) 1.024(3)	1.001(3) 1.000(2) 1.001(3)

	Predicted KIEs for $TS_{c\text{-}c}$				
DFT method	*C1*	*C2*	*C3*	*r(C-C) (Å)*	*Img. Freq*
B3LYP-D3(BJ)/6-31+G CPCM(DCE)*	1.052	1.039	1.000	1.92	-388.13
*B3LYP-D3(BJ)/6-31+G** CPCM(DCE)*	1.052	1.039	1.000	1.91	-394.40
*M06/6-31+G** CPCM(DCE)*	1.048	1.032	1.001	1.98	-310.45
*M062X/6-31+G** CPCM(DCE)*	1.050	1.037	1.003	1.92	-365.28
*wB97XD/6-31+G** CPCM(DCE)*	1.051	1.036	1.002	1.98	-391.01
*PBE0-D3(BJ)/6-31+G** CPCM(DCE)*	1.050	1.037	1.001	1.94	-376.88
*B97D-D3(BJ)/6-31+G** CPCM(DCE)*	1.045	1.034	1.001	1.82	-197.97
*PBE-D3(BJ)/6-31+G** CPCM(DCE)*	1.048	1.036	1.001	1.87	-259.32
B3LYP-D3(BJ)/def2-SVP CPCM(DCE)	1.050	1.037	1.001	1.87	-338.49
B3LYP-D3(BJ)/6-31+G LANL2DZ(Fe) CPCM(DCE)*	1.053	1.039	1.001	1.93	-418.91
M06/def2-SVP CPCM(DCE)	1.045	1.030	1.001	1.93	-247.45
M062X/def2-SVP CPCM(DCE)	1.049	1.036	1.003	1.87	-336.23
wB97XD/def2-SVP CPCM(DCE)	1.050	1.035	1.002	1.95	-374.98
PBE0-D3(BJ)/def2-SVP CPCM(DCE)	1.050	1.036	1.001	1.91	-384.64
B97D-D3(BJ)/def2-SVP CPCM(DCE)	1.037	1.024	1.001	1.77	-69.84
PBE-D3(BJ)/def2-SVP CPCM(DCE)	1.044	1.030	1.001	1.83	-167.64

Supplementary Table 3: ^{13}C predicted KIEs, C-C bond-distances (Å), and the imaginary vibrational mode for the key carbon-carbon bond-forming step (**TS_{C-C}**) employing various computational methods

Functional	Basis Set (CPCM)	Imag Freq	$r_{(C-C)}$ (Å)	C-1	C-2	C-3
B3LYP-D3(BJ)	6-31+G*	-388.13	1.92	1.052	1.039	1.000
B3LYP-D3(BJ)	6-31+G**	-394.40	1.91	1.052	1.039	1.001
M06-2X	6-31+G**	-365.28	1.92	1.050	1.037	1.003
M06	6-31+G**	-310.45	1.98	1.048	1.032	1.001
B97-D	6-31+G**	-197.97	1.82	1.045	1.034	1.001
ωB97X-D	6-31+G**	-391.01	1.98	1.051	1.036	1.002
PBE-D3(BJ)	6-31+G**	-259.32	1.87	1.048	1.036	1.001

Supplementary Table 4: ^{13}C predicted KIEs, C-O bond distances (Å), and the imaginary vibrational mode for the carbon-oxygen bond-forming step (**TS_{C-O}**) employing various computational methods

Functional	Basis Set (CPCM)	Imag Freq	$r_{(C3-O)}$ (Å)	C-1	C-2	C-3
B3LYP-D3(BJ)	6-31+G*	-67.87	2.25	1.011	0.991	1.019
B3LYP-D3(BJ)	6-31+G**	-83.35	2.24	1.008	0.990	1.021
M06-2X	6-31+G**	-270.01	2.18	1.006	0.990	1.036
M06	6-31+G**	-186.34	2.08	1.007	0.986	1.030
B97-D	6-31+G**	-68.23	2.18	1.009	0.990	1.020
ωB97X-D	6-31+G**	-189.02	2.18	1.007	0.989	1.031
PBE-D3(BJ)	6-31+G**	-72.70	2.37	1.009	0.991	1.019

Supplementary Table 5: ^{13}C predicted KIEs, C-O bond-distances (Å) and the imaginary vibrational mode for the carbon-oxygen bond-breaking step (**TS_{rev}**) employing various computational methods

Functional	Basis Set (CPCM)	Imag Freq	$r_{(C1-O)}$ (Å)	C-1	C-2	C-3
B3LYP-D3(BJ)	6-31+G*	-204.79	2.01	1.042	0.993	1.002
B3LYP-D3(BJ)	6-31+G**	-210.09	2.03	1.040	0.993	1.002
M06-2X	6-31+G**	-376.62	2.08	1.051	0.994	1.000
M06	6-31+G**	-265.06	2.02	1.045	0.991	1.000
B97-D	6-31+G**	-199.93	2.05	1.038	0.995	1.005
ωB97X-D	6-31+G**	-267.00	2.07	1.045	0.993	1.000
PBE-D3(BJ)	6-31+G**	-154.09	2.10	1.033	0.996	1.005

Supplementary Note 6. Ab initio molecular dynamics simulations

Born Oppenheimer *ab initio* molecular dynamics (AIMD) simulations were performed using the QUICKSTEP module of the CP2K 7.1 package.[12] The solvent-solute structure was modeled using

a cubic periodic cell of dimensions 25.0 Å × 25.0 Å × 25.0 Å containing complex **5** solvated with 50 dichloroethane (DCE) molecules. Atomic forces were estimated using density functional theory (DFT) calculations with the Perdew−Burke−Ernzerhof (PBE) exchange-correlation functional. We have chosen the pure functional rather than a hybrid functional (e.g. B3LYP) to reduce the computational cost for this large system. The Kohn−Sham orbitals were described with hybrid Gaussian/plane-wave basis functions. DZVP basis sets and a Goedecker−Teter−Hutter (GTH)[13] pseudopotential were employed for all atoms. The auxiliary plane-wave basis set was expanded up to a 280 Ry cutoff. The Grimme D3 dispersion correction was used to describe dispersion interactions. A convergence criterion of 10^{-6} Hartree was imposed for the ground-state energy. The atomic positions were propagated using the Born−Oppenheimer molecular dynamics (BOMD) scheme with a time step of 0.5 fs. The simulation temperature was controlled through a Nosé−Hoover thermostat with a time constant of 0.1 ps.

Supplementary Note 7. *Ab initio* Metadynamics study

Metadynamics simulations were performed at 298 K to obtain the free energy profile for the oxetane formation in the carbonyl olefin metathesis process. We used coordination numbers (CNs), given by

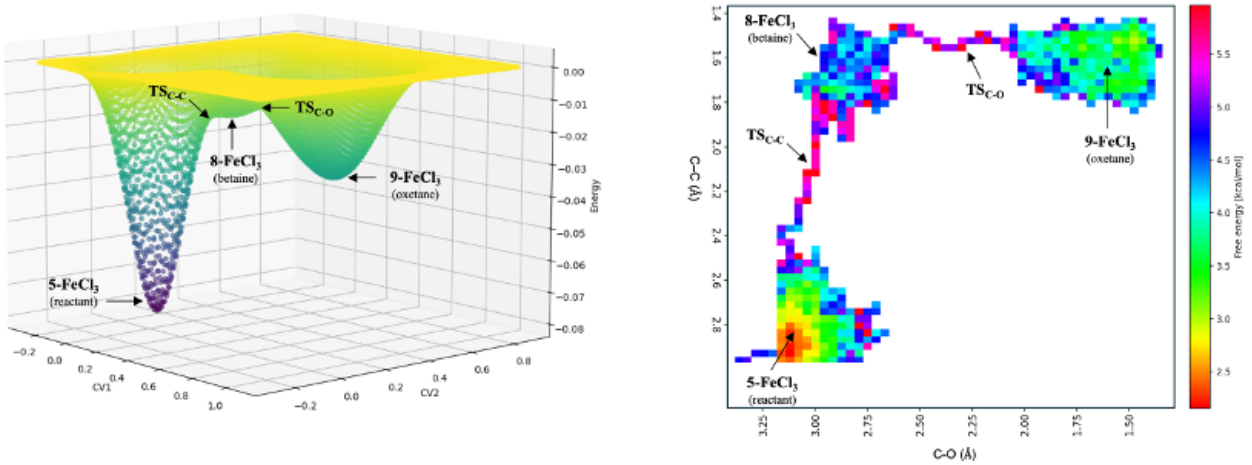
$$CN=[1-(d/d_0)^6]/\,[1-(d/d_0)^{12}]$$

where d is the distance between two atoms and d_0 is a reference distance, as collective variables (CVs). The reference distance (d_0) corresponding to CV1 and CV2 is 2.8 Å and 3.0 Å, respectively. The first collective variable, CV1, follows the bond formation between the carbonyl carbon (C1) and the styrene carbon (C2). The second collective variable, CV2, follows the bond formation between the carbonyl oxygen and the styrene carbon (C3), leading toward the formation of the oxetane intermediate. Repulsive Gaussian-shaped potential hills with a height of 0.6 kcal/mol and a width of 0.1 were added to the potential every 50 molecular dynamics steps for the two collective variables.

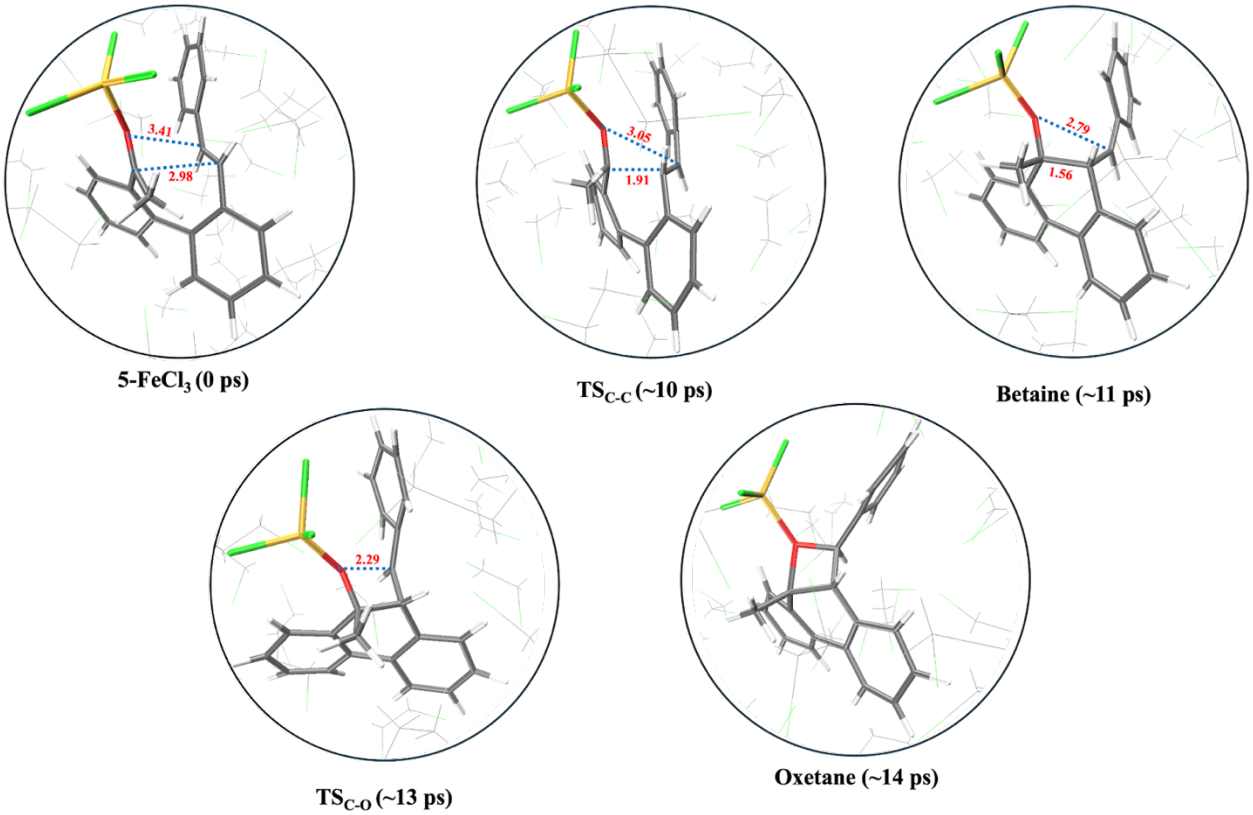
Supplementary Note 8. Free Energy Surface Calculations with *ab initio* Metadynamics

In this work, we employed AIMD simulations with a metadynamics approach for enhanced sampling of conformational space or rare events to understand the reaction mechanism. The AIMD

simulations can, therefore, be applied to find the intermediates, transition states, free energy surface, timing of bond formation or cleavage, stability, and lifetime of the intermediate species, which can't be predicted through static calculations. In our work, the primary goal of the AIMD metadynamics study is to map the free energy surface at the reaction temperature and identify the reactant, intermediate, and transition states and the stability of the intermediates (in our case, charge-separated betaine and four-membered oxetane). The starting point for the metadynamics simulation was determined by equilibrating **5** in the DCE solvent box (50 DCE molecules) for 3 ps, keeping the two styrenyl carbons (C2 and C3), carbonyl carbon, and oxygen constraints during the simulation. During the metadynamics simulations, we introduced a bias potential on the coordination number following the formation of C1−C2 and C3−O bonds, which were used as collective variables (**Supplementary Fig. 7**). A bias potential was added gradually to allow the entire free energy surface (FES), including the transition states and the different intermediate regions, to be sampled during the simulation. Therefore, this enhanced sampling method allows for exploring the carbonyl-olefin metathesis reaction pathways without prior knowledge of the landscape of the FES. The FES obtained using this procedure is shown in **Supplementary Fig. 7A**, and it is consistent with the experimental ^{13}C KIE measurement and static DFT studies that the cycloaddition reaction is stepwise *via* the formation of a metastable betaine intermediate. The free energy surface is shallow between the $TS_{C\text{-}C,}$ betaine intermediate, and the $TS_{C\text{-}O}$. Also, during the metadynamics simulation, the lifetime of the betaine intermediate is up to 2.0 ps timescale before going to the formation of $TS_{C\text{-}O.}$ The minimum energy path (MEP) on the surface (**Supplementary Fig. 7B**) indicates that the cycloaddition step is not concerted; rather, the reaction goes through the charge-separated betaine intermediate *via* C1-C2 bond formation and, finally, ring closing through C3-O bond formation, leading to the four-membered oxetane intermediate. The representative snapshot corresponds to the $TS_{C\text{-}C,}$ $TS_{C\text{-}O}$, betaine, and oxetane intermediate (**Supplementary Fig. 8**). Further looking into the FES, the $TS_{C\text{-}O}$ is 0.8 kcal/mol higher in energy compared to the $TS_{C\text{-}C.}$



Supplementary Figure 7. (A) *Ab initio* Metadynamics simulation of carbonyl olefin metathesis reaction in DCE solvent. **(B)** Free energy surface starting from the reaction complex five goes through the metastable betaine intermediate via C-C bond formation and, finally, ring closing by C-O bond formation to make the four-membered stable oxetane intermediate.

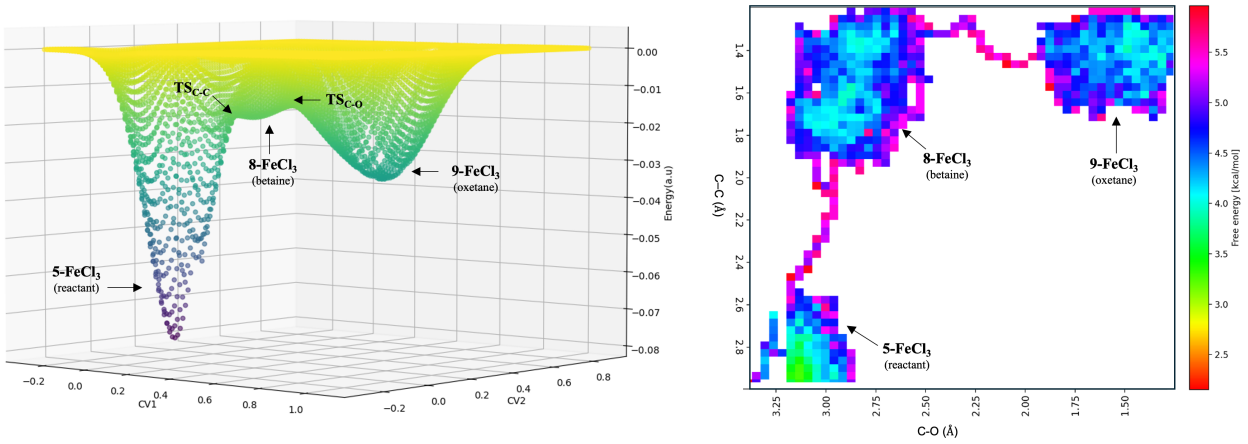


Supplementary Figure 8. Snapshots of the metadynamics trajectory starting from 5-FeCl$_3$ reactant complex the metastable betaine intermediate formed around 11.0 ps *via* TSc-c and finally the stable oxetane intermediate formed through ring-closing TSc-o around 13.0 ps dynamics timescale.

Identical results were obtained when we performed these AIMD metadynamics simulations in the absence of explicit solvent molecules, suggesting that the existence of the intermediate is not an artifact of the computational method and that the inclusion of solvent is not necessary to locate

the metastable betaine intermediate (See **Supplementary Fig. 9**). The metadynamics simulated free energy surface has been generated using the graph.psmp module of CP2K and our in-house Python code.

Therefore, the experimental KIEs, computational studies using static DFT, and *ab initio* metadynamics approach strongly support a stepwise mechanism *via* a betaine intermediate.

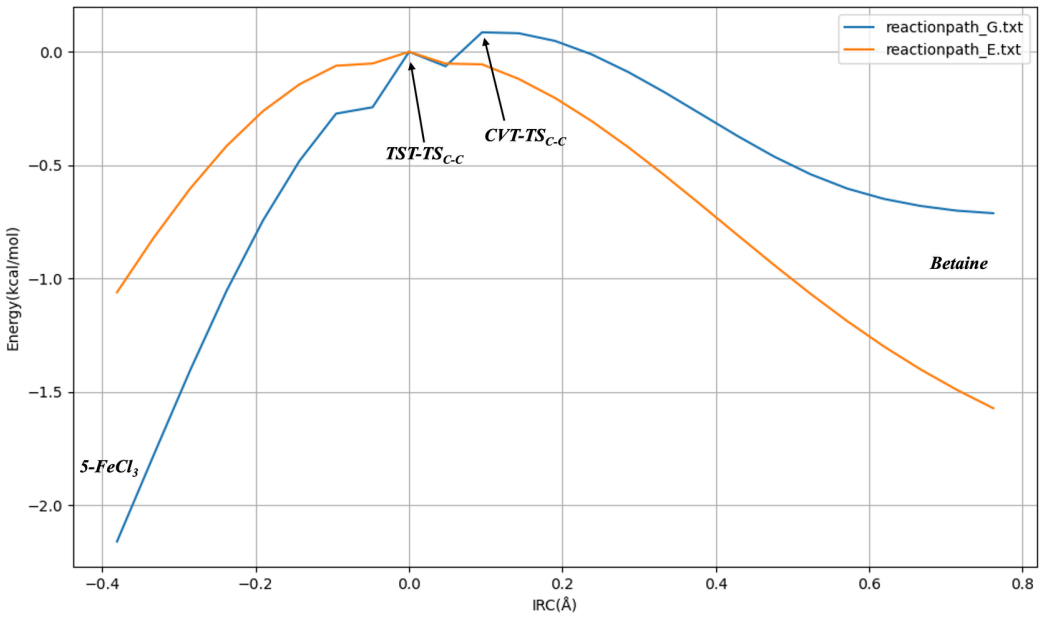


Supplementary Figure 9. (A) *Ab initio* Metadynamics simulation of carbonyl olefin metathesis reaction in the gas phase. **(B)** Free energy surface starting from the reaction complex five goes through the metastable betaine intermediate via C-C bond formation and, finally, ring closing by C-O bond formation to make the four-membered stable oxetane intermediate.

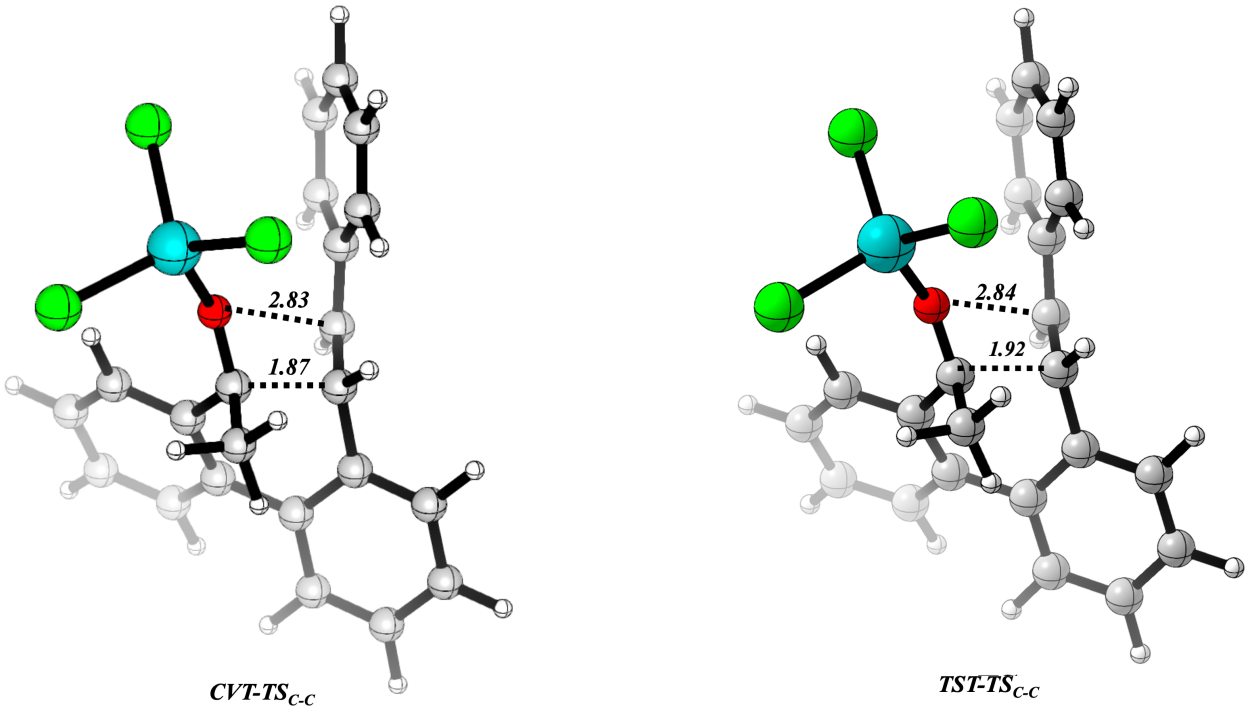
Supplementary Note 9. Canonical Variational Transition State (CVT) calculation

To address issues with the computation of entropic contribution in the free energy, CVT and associated reaction path calculations were carried out on the B3LYP-D3(BJ)/6-31+G* CPCM(DCE) potential energy surface using *Gaussrate* with the interface between *Polyrate17*[14] and *Gaussian16* with the application of the Reorientation of the Dividing Surface (RODS) algorithm, these are shown in **Supplementary Fig. 10**. For TS$_{C-C}$, CVT-TS differs from the PES TST-TS (comparison of the geometries for the CVT-TS with the conventional TST-TS is shown in **Supplementary Fig. 11**). The C_1–C_2 distance in CVT-TS$_{C-C}$ is 0.05 Å shorter than that in TST-TS$_{C-C}$, while the C_3–O distance in CVT-TS$_{C-C}$ is shorter than this in TST-TS$_{C-C}$ by 0.01 Å. It is worth mentioning that the CVT-TS$_{C-C}$ is geometrically quite similar to TST-TS$_{C-C}$ using B3LYP-D3(BJ)/6-311++G** CPCM(DCE) level of theory (shown in **Supplementary Fig. 12**). Also, the

CVT-$TS_{C\text{-}C}$ is higher in free energy by 0.13 kcal/mol than the corresponding TST-$TS_{C\text{-}C}$. As shown in **Supplementary Fig. 10**, this effect is an entropy effect. Note, however, that the difference in energy between the peaks of the free energy and potential energy curves is minimal (0.13 kcal mol^{-1}), consistent with flat surfaces, in terms of both potential energy and free energy, near the transition states. Also, we didn't locate an entropic intermediate in the reaction path.



Supplementary Figure 10. Reaction coordinate plots (B3LYP-D3(BJ)/6-31+G* CPCM(DCE)) for the betaine formation pathway. The locations of **CVT-TS** and **TST-TS** are highlighted.



Supplementary Figure 11. Geometries (B3LYP-D3(BJ)/6-31+G* CPCM(DCE)) of the canonical variational transition state and conventional transition state. Selected distances are shown in Å.

The canonical variational transition-state theory (CVTS) was used to calculate the rate constants for betaine formation from pre-reactive complex (5-$FeCl_3$), without tunneling, and the effect of multidimensional tunneling on the reaction dynamics was computed using the small-curvature tunneling (SCT) approximation. Further, the ^{13}C KIE was predicted (shown in Supplementary Table 6) for C_1, C_2, and C_3 from the unimolecular reaction rate calculated from polyrate.

Supplementary Table 6. Predicted ^{13}C KIE from the small curvature tunneling corrected canonical variational transition state.

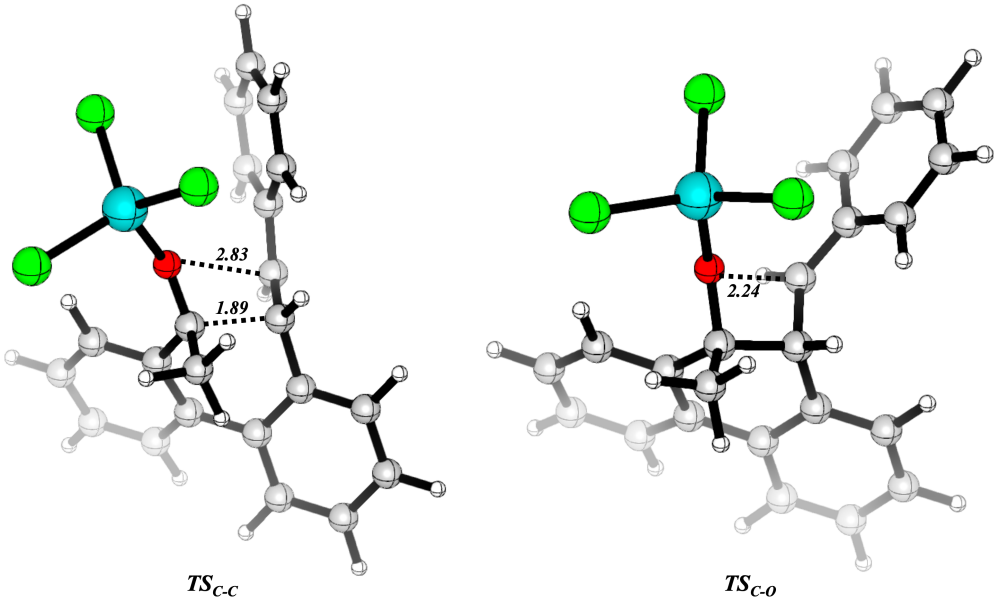
		^{13}C KIE				
Isotopic Center	TST	TST/w	TST/SCT	CVT	CVT/w	CVT/SCT
C_1	1.047	1.052	1.053	1.047	1.052	1.053
C_2	1.034	1.039	1.040	1.035	1.040	1.042
C_3	1.000	1.001	1.001	1.000	1.001	1.001

After refining the electronic energy using a larger basis set (6-311++G**), the harmonic free energy weighted KIE underestimated the experimentally measured KIE values both at the C1 and

C2 positions. Based on that, we decided to use the very high level (B3LYP-D3(BJ)/6-311++G** CPCM), (PBE-D3(BJ)/6-311++G** CPCM) and (M06/6-311++G** CPCM) geometry optimization (though it's computationally more demanding) and energy refinement, which might give the correct prediction of harmonic free energy weighted KIE based on both accurate geometry and energy. The results are given in Supplementary Table 7 and **Supplementary Fig. 12**. Though the geometry remains relatively unchanged, the relative energy changes and which makes the energy weighted KIE prediction using B3LYP-D3(BJ)/6-311++G** CPCM close to the experimentally measured values. On the other hand, the energy weighted KIE using PBE-D3(BJ)/6-311++G** CPCM goes in the wrong direction.

Supplementary Table 7: Harmonic free energy weighted ^{13}C predicted KIEs from TS_{CC} and TS_{CO} using very large basis set (6-311++G**) and density functionals (e.g, B3LYP, M06, and PBE) for geometry optimization and energy refinement.

Method	B3LYP-D3(BJ)/6-311++G** CPCM (solvent=DCE)				
					TScc-TSco
	C1	C2	C3	%TS	Kcal/mol
TS(C-C)	1.052	1.039	1.001	80.8	0.85
TS(C-O)	1.009	0.991	1.021	19.2	
weighted KIE	1.044	1.03	1.004		
Method	M06/6-311++G** CPCM (solvent=DCE)				
					TScc-TSco
	C1	C2	C3	%TS	Kcal/mol
TS(C-C)	1.049	1.033	1.001	78.9	0.78
TS(C-O)	1.007	0.986	1.029	21.1	
weighted KIE	1.04	1.023	1.007		
Method	PBE-D3(BJ)/6-311++G** CPCM (solvent=DCE)				
					TScc-TSco
	C1	C2	C3	%TS	Kcal/mol
TS(C-C)	1.046	1.034	1.001	24.7	-0.66
TS(C-O)	1.009	0.991	1.014	75.3	
weighted KIE	1.018	1.002	1.011		



Supplementary Figure 12: Lowest energy transition state geometries ($TS_{C\text{-}C}$ and $TS_{C\text{-}O}$) located at the potential energy surface using B3LYP-D3(BJ)/6-311++G** CPCM(DCE) level of theory.

The above result suggests that there is a role of dynamics in the ring-closing COM reaction, which can be captured through trajectory recrossing from quasiclassical dynamics using B3LYP-D3(BJ)/6-31+G* CPCM(DCE) level of theory, which overestimates the rate using conventional transition state theory.

Supplementary Note 10. AIMD downhill quasi-classical direct dynamics

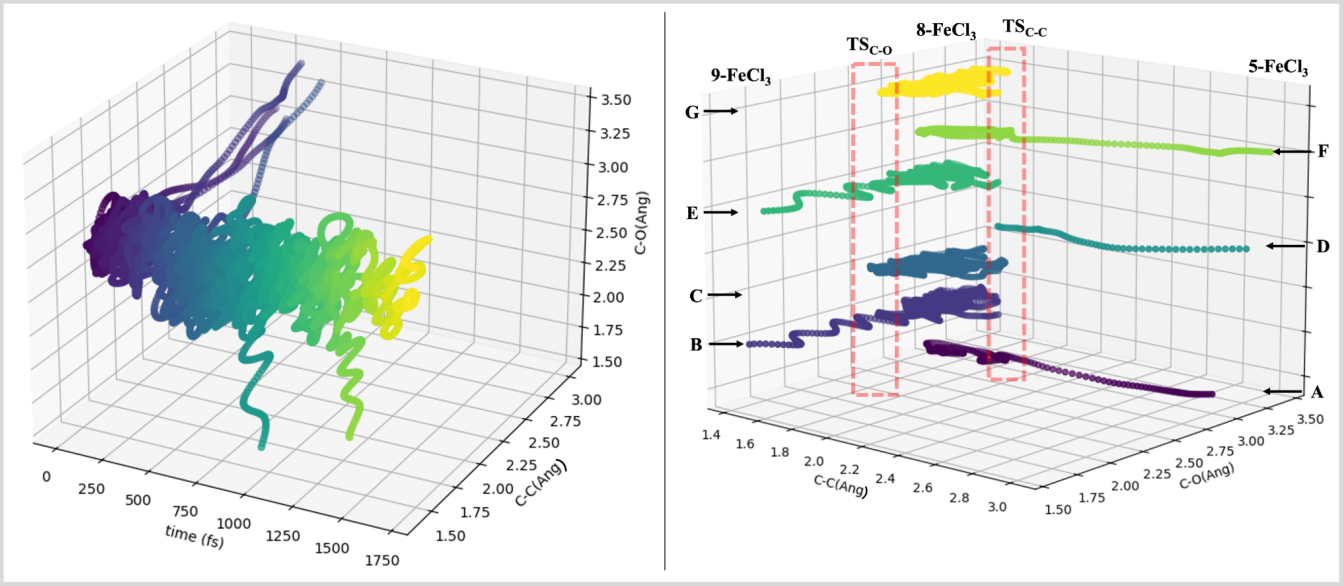
To explore the dynamic behavior of **$TS_{C\text{-}C}$**, **8**, and **$TS_{C\text{-}O}$**, the Progdyn script developed by Singleton[15] was employed. Trajectories were propagated with a 1.0 fs time step using the Verlet algorithm at the B3LYP-D3(BJ)/6-31+G* level at 298.15 K using the Gaussian16 C.01 version for quantum chemical calculations. The downhill quasi-classical (initiated at transition state **$TS_{C\text{-}C}$**) dynamics (with zero-point energy) trajectories were collected for further KIE analysis. To understand the nature of this stepwise mechanism *via* betaine intermediate and prediction of accurate KIEs with minimal assumptions, we calculated molecular trajectory in a 15Å cubic box starting from **$TS_{C\text{-}C}$** and were integrated forward and backward in time using quasi-classical dynamics until either **9** was formed or **5-$FeCl_3$** was re-formed. A total of 118 trajectories were obtained, and **Supplementary Fig. 13** illustrates representative examples of recrossing and productive trajectories. Out of 118 trajectories, 4 trajectories immediately recross to form **5-$FeCl_3$**,

22 were found as deep recross (completely form C-C (< 1.6 Å) bond then recross to **5-$FeCl_3$** within 250 fs), 11 trajectories traverse to **9,** and the remaining 81 stay at the betaine intermediate after 500 fs timescale. The trajectories that recross back to the **5-$FeCl_3$** happen within the first 250 fs timescale from the start of the direct dynamics. Here, we assume that the trajectories that formed the betaine intermediate **8** and stayed for more than 500 fs will eventually form the oxetane **9.** A second item of note is the agreement of the quasiclassical trajectories with the experimentally observed ^{13}C KIEs. That is, the proportion of trajectories that fully form the C–C bond and then recross (i.e., with reversible betaine formation) versus those that form oxetane **9** (22:92) can be used to weight the expected contributions of the $\mathbf{TS}_{c\text{-}o}$ versus $\mathbf{TS}_{c\text{-}c}$, respectively, to the overall observed KIE. Therefore, after analyzing the overall trajectory data, the contribution of $\mathbf{TS}_{c\text{-}o}$ and $\mathbf{TS}_{c\text{-}c}$ is 19.3% and 80.7%, respectively, towards the KIE prediction. When this is done, the overall KIEs (Supplementary Table 8) are in quite good agreement with the experimentally measured values.

Supplementary Table 8. Predicted and experimental ^{13}C KIEs. *a weighted by using the harmonic free energy difference in B3LYP-D3(BJ)/6-31+G* CPCM (DCE) level of theory (similar to Supplementary Fig. 5) *b weighted by using the harmonic free energy difference (similar to Supplementary Fig. 6) in B3LYP-D3(BJ)/6-311++G** CPCM (DCE)// B3LYP-D3(BJ)/6-31+G* CPCM (DCE) level of theory *c B3LYP-D3(BJ)/6-311++G** CPCM (DCE) level of theory *d weighted from the trajectories recrossing.

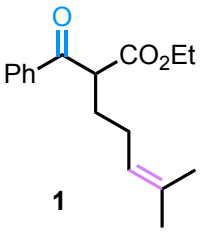
	^{13}C KIE		
Mechanism & Method	C_1	C_2	C_3
$TS_{c\text{-}c}$*(B3LYP-D3(BJ)/6-31+g*)*	*1.052*	*1.039*	*1.000*
$TS_{c\text{-}o}$*(B3LYP-D3(BJ)/6-31+g*)*	*1.011*	*0.991*	*1.019*
TS_{rev}*(B3LYP-D3(BJ)/6-31+g*)*	*1.042*	*0.993*	*1.002*
$TS_{c\text{-}c}/TS_{c\text{-}o}$ *weighted*[a]	*1.048*	*1.034*	*1.002*
$TS_{c\text{-}c}/TS_{c\text{-}o}$ *weighted*[b]	*1.040*	*1.025*	*1.006*
$TS_{c\text{-}c}/TS_{c\text{-}o}$ *weighted*[c]	*1.044*	*1.030*	*1.004*
$TS_{c\text{-}c}/TS_{c\text{-}o}$ *weighted*[d]	*1.044*	*1.029*	*1.003*
Experimental	*1.050(2)*	*1.027(4)*	*1.001(2)*
	1.050(3)	*1.027(4)*	*1.000(2)*
	1.048(3)	*1.024(3)*	*1.001(3)*

Note: the quasiclassical trajectories weighted KIE from ***B3LYP-D3(BJ)/6-31+g* CPCM(DCE)*** surface and the energy weighted KIE from ***B3LYP-D3(BJ)/6-311++G** CPCM (DCE)*** level of theory have quite good agreement with the experimentally measured average KIE.

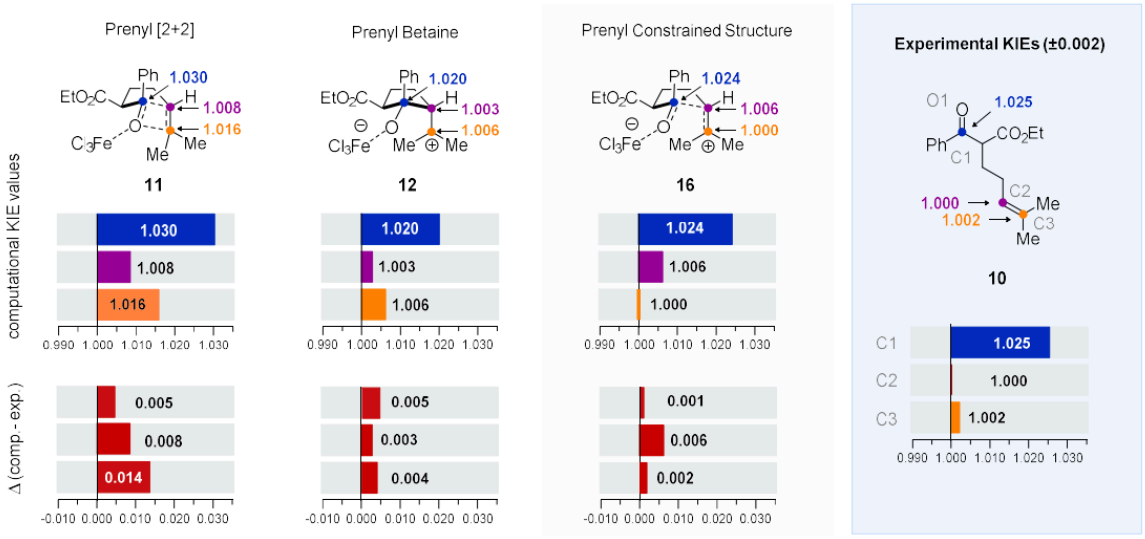


Supplementary Figure 13. The stacked plot of the paths for C–C and C–O bond formation in representative trajectories. A and F represent "deep recrossing", B and E represent "productive trajectories", C and G represent the formation of betaine intermediate and stable for ~2.0 ps, and D represents "immediate recrossing".

Supplementary Note 11. Comments on ^{13}C KIE interpretation Schindler and Kwan ChemRxiv 2022



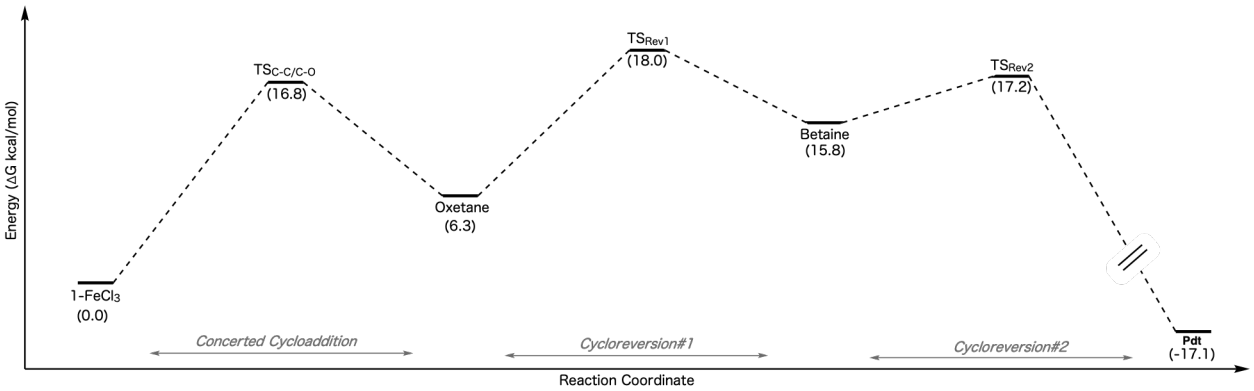
Reactant **1** in the manuscript has served as a benchmark substrate for the COM reaction. Prior mechanistic studies by Schindler, Zimmerman, and co-workers published in JACS (2017) focused on this type of substrate and concluded that oxetane formation occurs via a concerted, asynchronous [2+2] cycloaddition mechanism. Supplementary Ref. 16 (ChemRxiv, **November 3, 2022**. https://doi.org/10.26434/chemrxiv-2022-nnp81) describes a ^{13}C KIE study of reactant **1**, in which the authors measured a normal KIE of ~1.025 on the carbonyl carbon and negligible (close to 1.000) ^{13}C KIEs on the two olefin carbon atoms. See the graphic below, reproduced from the *ChemRxiv* article.



Supplementary Figure 14. (reproduced from Supplementary Ref. 16) Experimental ^{13}C KIEs for prenylated alkenes support a stepwise mechanism. Comparison of computational and experimental carbon KIEs. The KIEs do not match a concerted [2+2] transition state but are similar to the predicted EIEs for the first betaine. A closer match (16) to the experimental KIEs was found by considering structures with constrained C1–C2 and C3– O1 bond distances.

The authors suggest that these measurements are consistent with a stepwise mechanism for oxetane formation. This conclusion is based on the best match to a geometry-constrained prenyl intermediate of **1** that they claim represents a possible geometry for the first step of a stepwise mechanism. There are several issues with both the study and its interpretation; however, two main problems undermine the conclusions of this study. First, the experimental KIEs are not qualitatively (or quantitatively) consistent with the stepwise mechanism, and the constrained geometry is not representative of either step of the stepwise mechanism (there are known issues with KIE calculations from constrained systems that don't represent a saddle point on the surface and likely have issues with the vibrational frequencies). Second, calculations (by both Zimmerman and us, as shown below) demonstrate that the cycloreversion is turnover-limiting or co-turnover-limiting and would therefore contribute significantly to the KIE as the first irreversible step. Consequently, in the ChemRxiv study, the KIE is most likely reporting on the cycloreversion step and/or a combination of cycloreversion and oxetane formation. Based on these results and our own experimental KIE measurements, we determined that this was not a suitable experimental system to probe the mechanism of oxetane formation in the COM reaction.

Using computations, we investigated the prenyl substrate (**1**) in the ChemRxiv study using two different computational methods: B3LYP-D3(BJ)/6-31+G** CPCM (dichloroethane) and M062X/6-31+G** CPCM (dichloroethane). The free energy surfaces for these two methods are shown below in Supplementary Figs. 15 and 16.



Supplementary Figure 15. (A) Free energy profile for $FeCl_3$-catalyzed ring-closing COM of **1** calculated at B3LYP-D3(BJ)/6-31+G** CPCM (dichloroethane) // B3LYP-D3(BJ)/6-311++G** CPCM (dichloroethane) level of theory.

On the B3LYP-D3(BJ)/6-31+G** CPCM (dichloroethane) surface, the reaction proceeds via concerted oxetane formation followed by stepwise cycloreversion. All three transition structures lie within 1.2 kcal/mol of one another and therefore would all contribute to the predicted ^{13}C KIE, as shown below. *Note that the largest contributions to the KIEs come from the cycloreversion steps; therefore, the experimental KIE likely does not report on oxetane formation.*

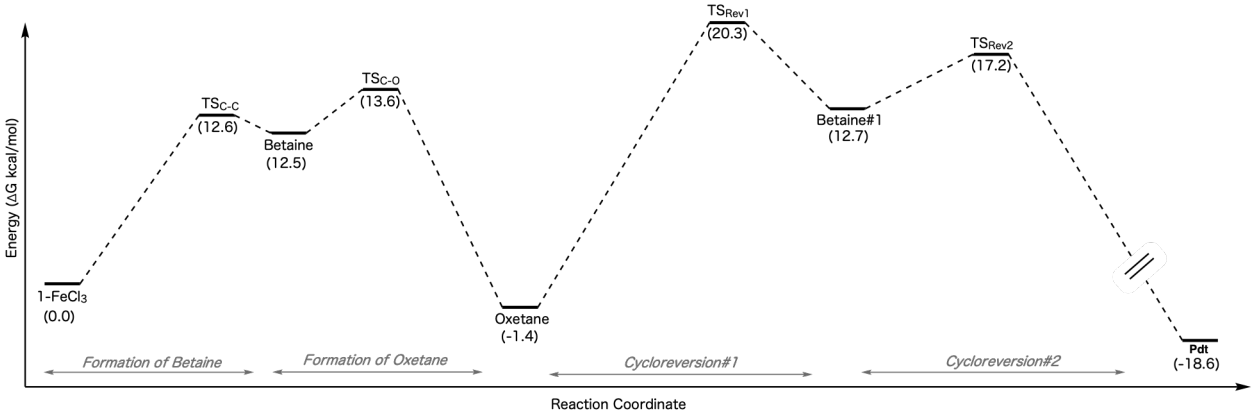
Comparison of experimental and predicted ^{13}C KIEs for B3LYP-D3(BJ)/6-31+G** CPCM (dichloroethane) calculations

Contribution of transition structures to the harmonic frequency weighted KIE predictions ($TS_{C\text{-}C/C\text{-}O}$ =8.0%; TS_{Rev1} = 61.0%; TS_{Rev2} =31.0 %).

	$TS_{C\text{-}C/C\text{-}O}$	TS_{Rev1}	TS_{Rev2}	Free energy-weighted KIEs	Exp
C1	1.025	1.023	1.009	1.019	1.025
C2	1.006	0.998	1.043	1.013	1.000
C3	1.019	1.008	1.047	1.021	1.002

Clearly, this is inconsistent with experiment. More importantly, this measurement does not probe the oxetane formation step exclusively.

The M062X/6-31+G** CPCM (dichloromethane) surface predicts a shallow betaine intermediate for oxetane and a turnover-limiting cycloreversion that occurs stepwise. Therefore, KIEs would reflect the first irreversible step, consistent with turnover-limiting cycloreversion. Once again, this surface does not probe oxetane formation. However, the predicted KIEs are qualitatively consistent with experiment, as shown below – with the C1 KIE being over-predicted. Notably, this reflects the cycloreversion step, not oxetane formation as reported in the preprint.



Supplementary Figure 16. (A) Free energy profile for $FeCl_3$-catalyzed ring-closing COM of **1** calculated at M062X/6-31+G** CPCM (dichloroethane) // M062X/6-311++G** CPCM (dichloroethane) level of theory.

Comparison of experimental and predicted ^{13}C KIEs for M062X/6-31+G** CPCM (dichloroethane) calculations

Contribution of transition states towards the harmonic frequency weighted KIE prediction (TS_{Rev1} = 99.45%; TS_{Rev2} =0.55 %)

	TS_{C-C}	TS_{C-O}	TS_{Rev1}	TS_{Rev2}	Free energy _weighted KIEs	Exp
C1	1.039	1.023	1.039	1.012	1.039	1.025
C2	1.032	1.008	1.000	1.039	1.000	1.000
C3	1.008	1.012	1.002	1.040	1.002	1.002

Supplementary Note 12. Free energy surfaces calculated using various DFT methods

This section includes the energies of all calculated structures with various levels of theory.

Supplementary Table 9. Energies of the geometries used for computing the potential energy surface for the $FeCl_3$ catalyzed COM reaction at B3LYP-D3(BJ)/6-31+G* CPCM (DCE) level of theory.

	E(a.u)	G_QRRHO	E+G_QRRHO	G(kcal/mol)
5	-3568.976121	0.283955	-3568.692166	-2239354.334
TS(C-C)	-3568.953818	0.286289	-3568.667529	-2239338.874
BETAINE	-3568.957984	0.287296	-3568.670688	-2239340.857
TS(C-O)	-3568.956599	0.287067	-3568.669532	-2239340.131
OXETANE	-3568.972159	0.289616	-3568.682543	-2239348.296
TS (cyclorev)	-3568.960777	0.28672	-3568.674057	-2239342.971
PDT1	-2990.042131	0.073157	-2989.968974	-1876205.531
PDT2	-578.9402825	0.186773	-578.7535095	-363167.8272
BETAINE1	-3568.959587	0.286366	-3568.673221	-2239342.446
OXETANE1	-3568.97216	0.289615	-3568.682545	-2239348.297

Supplementary Table 10. Energies of the geometries used for computing the potential energy surface for the $FeCl_3$ catalyzed COM reaction at PBE-D3(BJ)/6-31+G** CPCM (DCE) level of theory.

	E(a.u)	G_QRRHO	E+G_QRRHO	G(kcal/mol)
5	-3566.885256	0.274351	-3566.610905	-2238048.343
TS(C-C)	-3566.867363	0.275568	-3566.591795	-2238036.351
BETAINE	-3566.869141	0.275568	-3566.592626	-2238036.873
TS(C-O)	-3566.869023	0.276444	-3566.592579	-2238036.844
OXETANE	-3566.885364	0.279425	-3566.605939	-2238045.227
TS(cyclorev)	-3566.874675	0.27671	-3566.597965	-2238040.223
PDT1	-2988.731369	0.069372	-2988.661997	-1875385.403
PDT2	-578.1614082	0.180435	-577.9809732	-362683.0607
BETAINE1	-3566.870649	0.275938	-3566.594711	-2238038.181
OXETANE1	-3566.885522	0.278773	-3566.606749	-2238045.735

Supplementary Table 11. Energies of the geometries used for computing the potential energy surface for the $FeCl_3$ catalyzed COM reaction at M06/6-31+G** CPCM (DCE) level of theory.

	E(a.u)	G_QRRHO	E+G_QRRHO	G(kcal/mol)
5	-3568.033095	0.282121	-3567.750974	-2238763.736
TS(C-C)	-3568.011323	0.283202	-3567.728121	-2238749.396
BETAINE	-3568.016422	0.284617	-3567.731805	-2238751.708
TS(C-O)	-3568.015552	0.285251	-3567.730301	-2238750.764

OXETANE	-3568.033435	0.287625	-3567.74581	-2238760.495
TS (cyclorev)	-3568.019257	0.284969	-3567.734288	-2238753.266
PDT1	-2989.606652	0.072536	-2989.534116	-1875932.658
PDT2	-578.4353992	0.184935	-578.2504642	-362852.1663
BETAINE1	-3568.018351	0.284863	-3567.733488	-2238752.764
OXETANE1	-3568.033435	0.28764	-3567.745795	-2238760.486

Supplementary Table 12. Energies of the geometries used for computing the potential energy surface for the $FeCl_3$ catalyzed COM reaction at M06-2X/6-31+G** CPCM (DCE) level of theory.

	E(a.u)	G_QRRHO	E+G_QRRHO	G(kcal/mol)
5	-3568.305262	0.287008	-3568.018254	-2238931.454
TS(C-C)	-3568.284344	0.288625	-3567.995719	-2238917.313
BETAINE	-3568.289139	0.289209	-3567.99993	-2238919.956
TS(C-O)	-3568.285161	0.289071	-3567.99609	-2238917.546
OXETANE	-3568.311202	0.292869	-3568.018333	-2238931.504
TS (cyclorev)	-3568.289753	0.288843	-3568.00091	-2238920.571
PDT1	-2989.678364	0.07444	-2989.603924	-1875976.462
PDT2	-578.6367162	0.188037	-578.4486792	-362976.5462
BETAINE1	-3568.290376	0.288669	-3568.001707	-2238921.071
OXETANE1	-3568.311312	0.292294	-3568.019018	-2238931.934

Supplementary Table 13. Energies of the geometries used for computing the potential energy surface for the $FeCl_3$ catalyzed COM reaction at B97D/6-31+G** CPCM (DCE) level of theory.

	E(a.u)	ZPE(a.u)	E+ZPE(a.u)	G_QRRHO
5	-3568.697402	0.273095	-3568.424307	-2239186.253
TS(C-C)	-3568.675977	0.276233	-3568.399744	-2239170.839
BETAINE	-3568.676179	0.276761	-3568.399418	-2239170.635
TS(C-O)	-3568.674256	0.277548	-3568.396708	-2239168.934
OXETANE	-3568.686893	0.279303	-3568.40759	-2239175.763
TS(cyclorev)	-3568.678121	0.276274	-3568.401847	-2239172.159
PDT1	-2990.25468	0.067649	-2990.187031	-1876342.362
PDT2	-578.4485042	0.179626	-578.2688782	-362863.7211
BETAINE1	-3568.678208	0.276827	-3568.401381	-2239171.867
OXETANE1	-3568.686922	0.276827	-3568.408199	-2239176.145

Supplementary Table 14. Energies of the geometries used for computing the potential energy surface for the $FeCl_3$ catalyzed COM reaction at ωB97xD/6-31+G** CPCM (DCE) level of theory.

	E(a.u)	ZPE(a.u)	E+ZPE(a.u)	G_QRRHO

5	-3568.50538	0.286161	-3568.219219	-2239057.56
TS(C-C)	-3568.481199	0.289374	-3568.191825	-2239040.37
BETAINE	-3568.489668	0.290136	-3568.199532	-2239045.206
TS(C-O)	-3568.488047	0.290659	-3568.197388	-2239043.861
OXETANE	-3568.511067	0.292411	-3568.218656	-2239057.207
TS(cyclorev)	-3568.492525	0.290224	-3568.202301	-2239046.944
PDT1	-2989.817384	0.074187	-2989.743197	-1876063.856
PDT2	-578.6932394	0.1887	-578.5045394	-363011.5985
BETAINE1	-3568.491059	0.2899	-3568.201159	-2239046.227
OXETANE1	-3568.511037	0.293035	-3568.218002	-2239056.796

Supplementary Table 15. Energies of the geometries used for computing the potential energy surface for the $FeCl_3$ catalyzed COM reaction at B3LYP-D3(BJ)/6-31+G** CPCM (DCE) level of theory.

	E(a.u)	ZPE(a.u)	E+ZPE(a.u)	G_QRRHO
5	-3569.002889	0.283134	-3568.719755	-2239371.646
TS(C-C)	-3568.981249	0.285561	-3568.695688	-2239356.545
BETAINE	-3568.98529	0.28657	-3568.69872	-2239358.446
TS(C-O)	-3568.98383	0.286265	-3568.697565	-2239357.722
OXETANE	-3568.999042	0.289483	-3568.709559	-2239365.248
TS(cyclorev)	-3568.98795	0.285977	-3568.701973	-2239360.488
PDT1	-2990.051297	0.072916	-2989.978381	-1876211.434
PDT2	-578.9583991	0.186229	-578.7721701	-363179.5368
BETAINE1	-3568.986897	0.285629	-3568.701268	-2239360.046
OXETANE1	-3568.999289	0.2884	-3568.710889	-2239366.083

Supplementary Table 16. Energies of the geometries used for computing the potential energy surface for the $FeCl_3$ catalyzed COM reaction at B3LYP-D3(BJ)/6-311++G** CPCM (DCE)// B3LYP-D3(BJ)/6-31+G** CPCM (DCE) level of theory.

	E(a.u)	ZPE(a.u)	E+ZPE(a.u)	G_QRRHO	E+G_QRRHO	G(kcal/mol)
5	-3569.348806	0.338654	-3569.010152	0.283134	-3569.065672	-2239588.709
TS(C-C)	-3569.32599	0.338952	-3568.987038	0.285561	-3569.040429	-2239572.869
BETAINE	-3569.329139	0.340374	-3568.988765	0.28657	-3569.042569	-2239574.212
TS(C-O)	-3569.327603	0.339977	-3568.987626	0.286265	-3569.041338	-2239573.439
OXETANE	-3569.342925	0.342495	-3569.00043	0.289483	-3569.053442	-2239581.035
TS(cyclorev)	-3569.332081	0.339928	-3568.992153	0.285977	-3569.046104	-2239576.43
PDT1	-2990.293326	0.115562	-2990.177764	0.072916	-2990.22041	-1876363.307
PDT2	-579.0612484	0.222384	-578.8388644	0.186229	-578.8750194	-363244.0747
BETAINE1	-3569.330525	0.340286	-3568.990239	0.285629	-3569.044896	-2239575.672
OXETANE1	-3569.343264	0.342109	-3569.001155	0.2884	-3569.054864	-2239581.927

Supplementary Table 17. Energies of the geometries used for computing the potential energy surface for the $FeCl_3$ catalyzed COM reaction at B97D/6-311++G** CPCM (DCE)//B97D/6-31+G** CPCM (DCE) level of theory.

	E(a.u)	ZPE(a.u)	E+ZPE(a.u)	G_QRRHO	E+G_QRRHO	G(kcal/mol)
5	-3569.047895	0.329578	-3568.718317	0.273095	-3568.7748	-2239406.187
TS(C-C)	-3569.025202	0.330094	-3568.695108	0.276233	-3568.748969	-2239389.978
BETAINE	-3569.025143	0.33093	-3568.694213	0.276761	-3568.748382	-2239389.61
TS(C-O)	-3569.022929	0.331426	-3568.691503	0.277548	-3568.745381	-2239387.727
OXETANE	-3569.035835	0.332963	-3568.702872	0.279303	-3568.756532	-2239394.724
TS (cyclorev)	-3569.027057	0.330712	-3568.696345	0.276274	-3568.750783	-2239391.116
PDT1	-2990.499128	0.112549	-2990.386579	0.067649	-2990.431479	-1876495.753
PDT2	-578.5534351	0.216437	-578.3369981	0.179626	-578.3738091	-362929.5652
BETAINE1	-3569.02666	0.33146	-3568.6952	0.276827	-3568.749833	-2239390.52
OXETANE1	-3569.035784	0.332782	-3568.703002	0.278723	-3568.757061	-2239395.056

Supplementary Table 18. Energies of the geometries used for computing the potential energy surface for the $FeCl_3$ catalyzed COM reaction at M062X/6-311++G** CPCM (DCE)//M062X/6-31+G** CPCM (DCE) level of theory.

	E(a.u)	ZPE(a.u)	E+ZPE(a.u)	G_QRRHO	E+G_QRRHO	G(kcal/mol)
5	-3568.694596	0.341491	-3568.353105	0.287008	-3568.407588	-2239175.761
TS(C-C)	-3568.669911	0.341584	-3568.328327	0.288625	-3568.381286	-2239159.257
BETAINE	-3568.673893	0.342844	-3568.331049	0.289209	-3568.384684	-2239161.389
TS(C-O)	-3568.669871	0.342486	-3568.327385	0.289071	-3568.3808	-2239158.952
OXETANE	-3568.695893	0.345453	-3568.35044	0.292869	-3568.403024	-2239172.897
TS(cyclorev)	-3568.67491	0.342383	-3568.332527	0.288843	-3568.386067	-2239162.257
PDT1	-2989.950353	0.116754	-2989.833599	0.07444	-2989.875913	-1876147.135
PDT2	-578.7492345	0.224134	-578.5251005	0.188037	-578.5611975	-363047.1514
BETAINE1	-3568.675063	0.342739	-3568.332324	0.288669	-3568.386394	-2239162.463
OXETANE1	-3568.696085	0.345183	-3568.350902	0.292294	-3568.403791	-2239173.379

Supplementary Table 19. Energies of the geometries used for computing the potential energy surface for the $FeCl_3$ catalyzed COM reaction at M06/6-311++G** CPCM (DCE)//M06/6-31+G** CPCM (DCE) level of theory.

	E(a.u)	ZPE(a.u)	E+ZPE(a.u)	G_QRRHO	E+G_QRRHO	G(kcal/mol)
5	-3568.342479	0.336916	-3568.005563	0.282121	-3568.060358	-2238957.875
TS(C-C)	-3568.318961	0.336735	-3567.982226	0.283202	-3568.035759	-2238942.439

BETAINE	-3568.322921	0.338341	-3567.98458	0.284617	-3568.038304	-2238944.036
TS(C-O)	-3568.322197	0.338465	-3567.983732	0.285251	-3568.036946	-2238943.183
OXETANE	-3568.340889	0.340679	-3568.00021	0.287625	-3568.053264	-2238953.423
TS(cyclorev)	-3568.32632	0.338369	-3567.987951	0.284969	-3568.041351	-2238945.948
PDT1	-2989.817794	0.11509	-2989.702704	0.072536	-2989.745258	-1876065.149
PDT2	-578.5312757	0.221141	-578.3101347	0.184935	-578.3463407	-362912.3288
BETAINE1	-3568.324682	0.338734	-3567.985948	0.284863	-3568.039819	-2238944.986
OXETANE1	-3568.340888	0.340684	-3568.000204	0.28764	-3568.053248	-2238953.413

Supplementary Table 20. Energies of the geometries used for computing the potential energy surface for the $FeCl_3$ catalyzed COM reaction at ωB97xD/6-311++G** CPCM (DCE)// ωB97D/6-31+G** CPCM (DCE) level of theory.

	E(a.u)	ZPE(a.u)	E+ZPE(a.u)	G_QRRHO	E+G_QRRHO	G(kcal/mol)
5	-3568.839905	0.341717	-3568.498188	0.286161	-3568.553744	-2239267.474
TS(C-C)	-3568.814528	0.342526		0.289374	-3568.525154	-2239249.534
BETAINE	-3568.822055	0.343782	-3568.478273	0.290136	-3568.531919	-2239253.779
TS(C-O)	-3568.820429	0.343793	-3568.476636	0.290659	-3568.52977	-2239252.431
OXETANE	-3568.843594	0.345992	-3568.497602	0.292411	-3568.551183	-2239265.867
TS(cyclorev)	-3568.82533	0.343609	-3568.481721	0.290224	-3568.535106	-2239255.779
PDT1	-2990.052826	0.116741	-2989.936085	0.074187	-2989.978639	-1876211.596
PDT2	-578.7908423	0.224737	-578.5661053	0.1887	-578.6021423	-363072.8443
BETAINE1	-3568.823387	0.343993	-3568.479394	0.2899	-3568.533487	-2239254.763
OXETANE1	-3568.843571	0.346065	-3568.497506	0.293035	-3568.550536	-2239265.461

Supplementary Table 21. Energies of the geometries used for computing the potential energy surface for the $FeCl_3$ catalyzed COM reaction at B3LYP-D3(BJ)/6-311++G** CPCM (DCE)// B3LYP-D3(BJ)/6-31+G* CPCM (DCE) level of theory.

	E	E(kcal/mol)	G QRRHO	E+G QRRHO	G(kcal/mol)
5	-3569.348627	-2239766.264	0.27749439	-3569.071133	-2239592.136
TS(C-C)	-3569.325882	-2239751.991	0.28050722	-3569.045375	-2239575.973
BETAINE	-3569.331003	-2239755.205	0.28100243	-3569.050001	-2239578.876
TS(C-O)	-3569.327521	-2239753.019	0.28132058	-3569.0462	-2239576.491
OXETANE	-3569.343232	-2239762.878	0.28362151	-3569.05961	-2239584.905
TS(cyclorev)	-3569.33202	-2239755.842	0.28072467	-3569.051295	-2239579.688
PDT1	-2990.293205	-1876408.986	0.07073098	-2990.222474	-1876364.602
PDT2	-579.0613213	-363360.9791	0.185014345	-578.876307	-363244.8826

Supplementary Table 22. Energies of the geometries used for computing the potential energy surface for the $FeCl_3$ catalyzed COM reaction at PBE-D3(BJ)/6-311++G** CPCM (DCE)// PBE-D3(BJ)/6-31+G** CPCM (DCE) level of theory.

	E	E(kcal/mol)	G QRRHO	E+G QRRHO	G(kcal/mol)
5	-3567.250317	-2238449.574	0.26814929	-3566.982168	-2238281.31
TS(C-C)	-3567.231034	-2238437.474	0.26911761	-3566.961916	-2238268.602
BETAINE	-3567.233158	-2238438.806	0.26886552	-3566.964292	-2238270.093
TS(C-O)	-3567.231625	-2238437.845	0.26978381	-3566.961841	-2238268.555
OXETANE	-3567.248311	-2238448.315	0.27225654	-3566.976054	-2238277.474
TS (cyclorev)	-3567.237568	-2238441.574	0.27038483	-3566.967183	-2238271.907
PDT1	-2988.97936	-1875584.549	0.06676926	-2988.912591	-1875542.651
PDT2	-578.2768177	-362868.7031	0.178596729	-578.098221	-362756.6337

Supplementary Note 13. Progdyn.conf file

```
#This is the configuration file for PROGDYN.  This file is read by progdynstarterHP and
# the awk programs proggenHP, prog1stpoint, prog2ndpoint, and progdynb.
#The programs won't read anything past the first blank line,
#and this file must end with a blank line.
#The program has a number of default values but they are unlikely to be what you want.
#Do not delete lines - rather, comment out lines for unwanted options.
#The values here are read repeatedly and most can be changed in the middle of running jobs
#***The keywords are case sensitive.  The following keywords should always be defined:***
#***method, charge, multiplicity, memory, processors, title
#*** method --The following word is copied exactly to the gaussian input file.
method b3lyp/6-31+g*
#To do a nonstandard route, make nonstandard 1.  For normal calcs, use nonstandard 0 or else leave it out.
#Then make a file called "nonstandard" containing the nonstandard route with no extra lines.
nonstandard 0
# NMRoptions As is NMRtype=1 will add a section for an NMR calc at every NMRevery intervals.  If you want to combine the two use nonstandard
#NMRtype 1
#NMRmethod2 B97D/6-31G*
#NMRmethod LC-wPBE/6-31G*
#NMRmethod3 B3LYP/cc-pvtz
#NMRevery 4
#NMRrand 1
#NMRcc 1
#loadlimit 10.0
#geometry linear
rotationmode 1
#*** method2 --The options here are restricted, unrestricted, and read. restricted is the default
#If the method is U..., put unrestricted here and the .com files will have in them guess=mix.
#If you put read here, the .com files will contain guess=tcheck, which sometimes makes things faster, sometimes not.
#The use of read requires a specifically defined checkpoint file name using the keyword checkpoint.
#method2 read
charge 0
multiplicity 6
#oniomchargemult 1 1
```

```
processors 16
#*** memory --The following "word" is copied exactly to the gaussian input file after %mem=.
memory 10gb
#*** killcheck and checkpoint -- You can use a specifically defined checkpoint file name by putting
#the name after the keyword checkpoint.  This is necessary if you use the read option with method2.
#Defined checkpoint names are an unnecessary modest hastle and if you do not want to bother, use killcheck 1
killcheck 0
checkpoint g16.chk
#*** diagnostics -- 0 prints out nothing extra, 1 (default) prints out extra stuff to a
#file "diagnostics", 2 adds more stuff, 3 adds velocities to a file "vellist"
#4 adds the apparent temperature to vellist, but this is meaningless with quasiclassical calculations
diagnostics 0
#*** title -- the title keyword must be followed by exactly four words
title olemet_b3lyp ub3lyp631+g* trial 298
#*** initialdis -- 0 (default) turns off displacement of the normal modes, so that all trajectories start from the same
place
# and only the energies and signs of the motion in the modes are randomized
# 1 gives a flat distribution of displacements where all of the possible values are equally likely
# 2 (recommended) gives a QM-like gaussian distribution of displacements, so that displacements in the middle are
more likely that
# those at the end by 1/e
initialdis 0
#initialdis 4 #what does 4 do? this was on before
#*** timestep -- this is the time between points in the trajectory.  Typical values would be 1E-15 or 0.5E-15 or 0.25E-
15
timestep 1E-15
#*** scaling -- this lets you scale the gaussian frequencies by a constant
scaling 0.9614
temperature 298
#*** thermostat 1 puts in a damping factor so as to bring the classical temperature toward the desired temperature.
#*** use a thermostatmult between 0.95 and 1, typically 0.995, so the damping happens slowly - otherwise there will
be
#*** overadjustment in response to random variation
#*** the thermostat is not exact.  The second traj point ignores this, so it only applies to later points handled by
progdynb.
#thermostat 1
#thermostatmult 0.995
#*** method3, method4, method5, and method6 -- These keywords let you add extra lines to the gaussian input file.
#method3 and method4 add lines at the top of the input after the lines defining the method, and
#this is useful to implement things like the iop for mPW1k
#method5 and method6 add lines after the geometry, after a blank line of course
#only a single term with no spaces can be added, one per method line.  Here are some examples to uncomment if
needed
#method3 IOp(3/76=0572004280)
method3 scrf=(cpcm,solvent=dichloroethane)
#method3  scrf=(solvent=chloroform)
#add the line below with big structures to get it to put out the distance matrix and the input orientation
method4 empiricaldispersion=gd3bj
#method4 int(finegrid)
#method4 scf=(conver=5)
#method4 iop(3/124=3)
#method4 scrf=(pcm,solvent=dmso,read)
#method5 radii=bondi
#method6
#*** methodfile -- This keyword lets you add more complicated endings to gaussian input files
#such as a gen basis set.  Put after the keyword the number of lines in a file you create called
```

```
#methodfile that contains the test you want to add to the end of the gaussian input
methodfile 0
#*** numimag --This tells the program the number of imaginary frequencies in the starting structure.
#if 0, treats as ground state and direction of all modes is random
#if 1, motion along the reaction coordinate will start out in the direction defined by searchdir
#if 2, only lowest freq will go direction of searchdir and other imag mode will go in random direction
numimag 1
#*** searchdir -- This keyword says what direction to follow the mode associated with the imaginary frequency.
#The choices are "negative" and "positive".  Positive moves in the direction defined in the gaussian frequency calculation
#for the imaginary frequency, while negative moves in the opposite direction.  The correct choice can be made either
#by a careful inspection of the normal modes and standard orientation geometry, or by trial and error.
searchdir  negative
#*** classical --  for quassiclassical dynamics, the default, use 0.  for classical dynamics, use 1
#if there are no normal modes and the velocities are to be generated from scratch, use classical 2
classical 0
#*** DRP, saddlepoint, and maxAtomMove --to run a DRP use 'DRP 1' in the line below, otherwise leave it at 0 or comment it out
#the treatment of starting saddlepoints is not yet implemented so use saddlepoint no
#if DRP shows oscillations then decrease maxAtomMove
#DRP 1
#saddlepoint no
#maxAtomMove 0.01
#*** cannonball -- The program can "fire" a trajectory from a starting position toward a particular target, such as toward
#a ts.  To use this, make a file cannontraj with numAtom lines and three numbers per line that defines the vector
#for firing the trajectory, relative to the starting geometry's standard orientation.  The number following cannonball sets
#the extra energy being put into the structure in kcal/mol
#cannonball 10
#*** keepevery --This tells the program how often to write the gaussian output file to file dyn, after the first two points.
#Use 1 for most dynamics to start with, but use a higher number to save on disk space or molden loading time.
keepevery 1
#*** highlevel --For ONIOM jobs, the following line states the number of highlevel atoms,
#which must come before the medium level atoms.  Use some high value such as 999 if not using ONIOM
highlevel 9999
#*** fixedatom1, fixedatom2, fixedatom3, and fixedatom4 - These fix atoms in space.
#Fixing one atom serves no useful purpose and messes things up, while fixing two atoms
#fixes one distance and fixing three has the effect of fixing three distances, not just two
#in current form fixed atoms only are meant to work with no displacements, that is, initialdis=0
#fixedatom1 16
#fixedatom2 1
#fixedatom3 4
#fixedatom4 20
#applyforce 1 lets one push atoms together or appart - a positive force pushes them together
#format is applyforce force    - with the units on force the same as in the Gaussian output file
#applyforce 2 or 3 or 4 applys a polynomical force centered at dist0.  2 is just harmonic, 3 is second order, 4 is third order
#format is applyforce 4 forcecoefficient dist0 forcecoefficient2 forcecoefficient3
#then use afatoms to chose the atoms with format afatoms firstatom secondatom [additional atoms]
#applyforce 2 0.1 2.0
#afatoms 5 11
#applyforceB 2 0.1 2.6
#afatomsB 6 9
#applyforceC 2 0.01 5.2
```

#afatomsC 8 15
#zeroatom pushes the numbered atom toward the origin with a small harmonic potential - good with boxon when you want to keep the reaction in the center
#zeroatom 16
#*** boxon and boxsize - With boxon 1, a cubic box is set such that atoms that reach the edge
#are reflected back toward the middle. Useful for dynamics with solvent molecules. This is a crude
#implementation that is ok for a few thousand femtoseconds but will not conserve energy long term.
#Set the box size so as to fit the entire initial molecule but not have too much extra room.
#The dimensions of the box are two times the boxsize, e.g. boxsize 7.5 leads to a box that is 15 x 15 x 15 angstroms
boxon 1
boxsize 7.5
#*** sphereon and spheresize and sphereforce - uses a force to push atoms within a sphere. notice that if the atom is far outside of
#the sphere then the force is large unless sphereforce is set small
#sphereon 1
#spheresize 12.9
#sphereforce .01
#setting a value for empiricaldispersion sets its s6 value with the Grimme 2006 algorithm. Default is 0, with no empiricaldispersion
#empiricaldispersion 1.0
#*** displacements -- This keyword lets you set the initialdis of particular modes by using a series of lines of the format
displacements NumberOfMode InitialDisForThatMode, as in the example below. You should be able to do as many of these as you like
you might consider this for rotations where a straight-line displacement goes wrong at large displacements
The choices for InitialDisForThatMode are 0, 1, 2, and 10, where 10 does the same thing as 0 but is maintained for now because
a previous version of the program had a bug that made 0 not work.
#displacements 2 0
#displacements 3 0
#*** etolerance --This sets the allowable difference between the desired energy in a trajectory and the actual
#energy, known after point 1 from the potential energy + the kinetic energy in the initial velocities.
#The unit is kcal/mol and 1 is a normal value for mid-sized organic systems. For very large and floppy molecules, a larger value
#may be needed, but the value must stay way below the average thermal energy in the molecule (not counting zpe).
#If initialdis is not 0 and few trajectories are being rejected, decrease the value.
etolerance 1
#*** controlphase --It is sometimes useful to set the phase of particular modes in the initialization of trajectories.
#The format is controlphase numberOfModeToControl positive or controlphase numberOfModeToControl negative.
#controlphase 2 positive
#*** damping -- The damping keyword lets you add or subtract energy from the system at each point, by multiplying the velocities
#by the damping factor. A damping of 1 has no effect, and since you mostly want to change the energy slowly, normal values range
#from 0.95 to 1.05. The use of damping lets one do simulated annealing - you add energy until the structure is moving enough
#to sample the kinds of possibilities you are interested in, then you take away the energy slowly.
damping 1.000
#at a damping of .9995, the energy is cut in half in 693 points
#*** reversetraj --This keyword sets the trajectories so that both directions from a transition state are explored.
reversetraj false
#updated Aug 9, 2007 to include the possibility of classical dynamics by the keyword classical
#updated Jan 2008 to include fixed atoms, ONIOM jobs, keepevery, and box size
#update Feb 2008 to include methodfile parameter
updated Nov 2008 to allow for start without an initial freq calc using classical = 2
update Aug 2010 to include etolerance, damping controlphase and reversetraj

Supplementary Note 14. CP2K metadynamics input file

```
&GLOBAL
  PROJECT olefin_metathesis
  RUN_TYPE MD
  PRINT_LEVEL MEDIUM
&END GLOBAL

&FORCE_EVAL
  METHOD QS
  STRESS_TENSOR ANALYTICAL
&DFT
    BASIS_SET_FILE_NAME BASIS_MOLOPT
    POTENTIAL_FILE_NAME GTH_POTENTIALS
    CHARGE 0
    LSD
    MULTIPLICITY 6
    &MGRID
      CUTOFF 280
      NGRIDS 5
    &END MGRID
    &QS
      METHOD GPW
      EXTRAPOLATION ASPC
      EPS_DEFAULT 1.0E-12
    &END QS
&POISSON
       PERIODIC XYZ
       POISSON_SOLVER PERIODIC
    &END
    &SCF
      MAX_SCF 500
#    SCF_GUESS ATOMIC
     SCF_GUESS RESTART
      EPS_SCF 1.0E-6
      &OUTER_SCF
        MAX_SCF 20
        EPS_SCF 1.0E-6
      &END OUTER_SCF
      #ADDED_MOS 200
      #EPS_SCF 5.0E-7 # default value 1.0E-5
      #CHOLESKY INVERSE
      #&SMEAR  ON
      #  METHOD FERMI_DIRAC
      #  ELECTRONIC_TEMPERATURE [K] 100
      #&END SMEAR
      #&DIAGONALIZATION
      #  ALGORITHM STANDARD
      #&END DIAGONALIZATION
      #&MIXING
      #  METHOD BROYDEN_MIXING
      #  ALPHA   0.1
      #  BETA    1.5
      #  NBROYDEN  8
```

```
    #&END MIXING
    &OT
      MINIMIZER DIIS
      PRECONDITIONER FULL_KINETIC
      ENERGY_GAP 0.001
    #  STEPSIZE 0.01
    &END OT
   &END SCF
   &XC
    &XC_FUNCTIONAL
   &PBE
    PARAMETRIZATION ORIG
   &END PBE
    &END XC_FUNCTIONAL
   &VDW_POTENTIAL
    POTENTIAL_TYPE PAIR_POTENTIAL
    &PAIR_POTENTIAL
     TYPE DFTD3
     REFERENCE_FUNCTIONAL PBE
     R_CUTOFF 16
     PARAMETER_FILE_NAME   dftd3.dat
     &END PAIR_POTENTIAL
   &END VDW_POTENTIAL
  &END XC
 &END DFT
 &PRINT
 &END PRINT

 &SUBSYS
  &CELL
    ABC 20.000 20.000 20.000
    ALPHA_BETA_GAMMA 90.0000 90.000 90.0000
#    PERIODIC XYZ
  &END CELL

  &TOPOLOGY
    COORD_FILE_FORMAT XYZ
    COORD_FILE_NAME olemet.xyz
  &END TOPOLOGY


  &KIND O
    BASIS_SET DZVP-MOLOPT-SR-GTH
    POTENTIAL GTH-PBE-q6
  &END KIND
  &KIND H
    BASIS_SET DZVP-MOLOPT-SR-GTH
    POTENTIAL GTH-PBE-q1
  &END KIND
  &KIND C
    BASIS_SET DZVP-MOLOPT-SR-GTH
    POTENTIAL GTH-PBE-q4
  &END KIND
  &KIND Fe
    BASIS_SET DZVP-MOLOPT-SR-GTH
    POTENTIAL GTH-PBE-q16
```

```
    &END KIND
    &KIND Cl
      BASIS_SET DZVP-MOLOPT-SR-GTH
      POTENTIAL GTH-PBE-q7
    &END KIND
&COLVAR
&COORDINATION
ATOMS_FROM 23 # C1
ATOMS_TO 37 # CO
R_0 3.0
&END COORDINATION
&END COLVAR
&COLVAR
&COORDINATION
ATOMS_FROM 21 # O
ATOMS_TO 22 # C2
R_0 2.8
&END COORDINATION
&END COLVAR
  &END SUBSYS
&END FORCE_EVAL
&MOTION
&MD
ENSEMBLE NVT
STEPS 50000
TIMESTEP 0.5
&THERMOSTAT
TYPE NOSE
&NOSE
LENGTH 3
YOSHIDA 3
MTS 2
TIMECON 100.00
&END NOSE
&END THERMOSTAT
TEMPERATURE 298.0
&END MD
&FREE_ENERGY
    &METADYN
      DO_HILLS
      NT_HILLS 50
      WW 1.0e-3
      WELL_TEMPERED
      DELTA_T 10000
      &METAVAR
        SCALE 0.1
        COLVAR 1
      &WALL
POSITION 0.015
TYPE REFLECTIVE
&REFLECTIVE
DIRECTION WALL_MINUS
&END REFLECTIVE
&END WALL
      &END METAVAR
      &METAVAR
```

```
      SCALE 0.1
      COLVAR 2
&WALL
POSITION 0.015
TYPE REFLECTIVE
&REFLECTIVE
DIRECTION WALL_MINUS
&END REFLECTIVE
&END WALL
    &END METAVAR
&PRINT
      &COLVAR
        COMMON_ITERATION_LEVELS 3
      &END
      &HILLS
        COMMON_ITERATION_LEVELS 3
      &END
#         &EACH
#           MD 1
#         &END
    &END
   &END METADYN
  &END
&PRINT
&RESTART
BACKUP_COPIES 0
&EACH
MD 1
&END EACH
&END RESTART
&RESTART_HISTORY
&EACH
MD 0
&END EACH
&END RESTART_HISTORY
&END PRINT
&END MOTION
&EXT_RESTART
EXTERNAL_FILE     olefin_metathesis.restart
RESTART_THERMOSTAT .TRUE.
RESTART_POS       .TRUE.
RESTART_VEL       .TRUE.
RESTART_COUNTERS  .TRUE.
&END
```

Supplementary Note 15. Gaussrate sample Input File:

Job.dat

*General

TITLE

5-$FeCl_3$ -> Betaine: B3LYP/6-31+G* (with coordinate from individual optimization using Gaussrate).

END

ATOMS

1	C
2	C
3	C
4	C
5	C
6	C
7	C
8	C
9	C
10	C
11	C
12	C
13	C
14	C
15	C
16	C
17	C
18	C
19	C
20	C
21	C
22	C
23	O
24	Fe
25	Cl
26	Cl
27	Cl
28	H
29	H
30	H
31	H
32	H
33	H
34	H
35	H
36	H
37	H
38	H
39	H
40	H
41	H
42	H
43	H

```
44      H
45      H
END

  NOSUPERMOL
  INPUNIT AU
  WRITEFU31  ON
  MDMOVIE ON

*OPTIMIZATION

  OPTMIN  OHOOK
  OPTTS   OHOOK

*SECOND

  HESSCAL    HHOOK

*REACT1

  INITGEO  GEOM
  STATUS   2

  GEOM
   1        4.60512142     7.78787492    -1.74170330
   2        4.50937860     5.47529364    -3.02459913
   3        2.30506025     4.03853090    -3.01762632
   4        0.13602459     4.88455112    -1.72619561
   5        0.26712165     7.19992456    -0.42269484
   6        2.47351449     8.64379618    -0.43740594
   7       -2.20783905     3.42150736    -1.61028669
   8       -2.76986977     1.34556937    -2.97566386
   9       -5.05416982    -0.22178194    -2.70961487
  10       -6.26013607    -0.74187003    -0.36950200
  11       -8.46820046    -2.21123633    -0.34488976
  12       -9.45994879    -3.23939432    -2.55917370
  13       -8.22972352    -2.80784975    -4.85527672
  14       -6.05592645    -1.32370475    -4.91142513
  15       -5.25142166     0.14739824     2.10017453
  16       -6.81115821     1.58623046     3.67933252
  17       -5.91562923     2.59937253     5.94595131
  18       -3.40067622     2.23855220     6.66558356
  19       -1.80905735     0.82735210     5.12252942
  20       -2.72399361    -0.28049072     2.88473812
  21       -0.93842038    -1.84060097     1.44715398
  22       -1.66973911    -4.24446793     0.16103405
```

```
  23        1.34694040    -1.18041027     1.49046259
  24        4.62823768    -2.44007826     0.28936499
  25        4.80569604    -6.37326952     1.71940415
  26        7.41902698     0.02534891     2.18196296
  27        4.99777599    -2.41029108    -3.87139566
  28       -8.73442386     1.97075953     3.08242736
  29        0.14175260     0.50630505     5.65790773
  30       -2.68985142     3.04605672     8.41001110
  31       -7.17645701     3.70252951     7.12896055
  32       -9.36871832    -2.61100971     1.45440956
  33       -5.11151084    -0.97217726    -6.69954174
  34      -11.15266230    -4.39441750    -2.48370908
  35       -8.95932481    -3.61987676    -6.59171339
  36       -3.57694063     4.09920726    -0.23701613
  37        2.29260271     2.22836120    -3.97491953
  38       -1.38168732     7.86226810     0.60655462
  39        6.16719476     4.77754608    -4.01160259
  40        2.53180766    10.42689360     0.57595720
  41        6.33009425     8.89813289    -1.74422850
  42       -1.47520604     0.73454582    -4.45209510
  43       -1.19745999    -4.14249354    -1.84948750
  44       -0.49585878    -5.74092527     0.98109991
  45       -3.65740470    -4.70413113     0.38764266
END

 SPECIES   NONLINRP

 ELEC
  6   0.0
 END

*PROD1

 INITGEO  GEOM
 STATUS   2

 GEOM
  1        5.06509385     7.09680888     2.51851188
  2        4.74407039     6.00239974     0.12191259
  3        2.50797304     4.79740866    -0.46161177
  4        0.54664762     4.63493662     1.38899216
  5        0.91287974     5.78532191     3.80703848
  6        3.15494296     6.99611095     4.35834209
  7       -1.64891554     3.24339283     0.99309300
  8       -2.27057204     1.73292965    -1.24714803
  9       -5.10060730     1.71708925    -1.68874706
```

```
  10       -6.62052240    -0.00810227    -0.34529784
  11       -9.23085991     0.00219433    -0.80684164
  12      -10.30287430     1.71103527    -2.50068649
  13       -8.78181927     3.43990984    -3.78640111
  14       -6.17813526     3.43433843    -3.37254598
  15       -5.42305421    -1.78096294     1.45823646
  16       -6.81438818    -2.96553900     3.38120227
  17       -5.67201714    -4.66853300     5.03137746
  18       -3.10155908    -5.20821491     4.79504400
  19       -1.68409531    -4.01825415     2.91775749
  20       -2.81581824    -2.30457436     1.26767026
  21       -1.23900185    -1.08193767    -0.81592871
  22       -1.52054763    -2.53886120    -3.31175491
  23        1.27091941    -0.89361774    -0.09942592
  24        4.41748866    -1.92237760    -0.90654091
  25        4.47614096    -6.17879181    -0.99371681
  26        7.13942075    -0.45967316     2.02539251
  27        5.40762617    -0.31836316    -4.75422487
  28       -8.80354398    -2.52683019     3.61309948
  29        0.31592269    -4.41166594     2.71866711
  30       -2.19659891    -6.53189771     6.07550934
  31       -6.78670890    -5.55990923     6.50562884
  32      -10.43542470    -1.36384647     0.13348625
  33       -4.96910590     4.75981856    -4.37098420
  34      -12.32857890     1.67915004    -2.82576550
  35       -9.60892271     4.77030442    -5.11065695
  36       -2.99570019     3.16465963     2.54583278
  37        2.26337234     3.94386928    -2.30348164
  38       -0.58459800     5.65888385     5.20231243
  39        6.25316411     6.09883506    -1.25930298
  40        3.45134638     7.85433651     6.19459699
  41        6.83048468     8.04455597     2.95869522
  42       -1.27721555     2.43041642    -2.91392650
  43       -0.38395908    -1.63909918    -4.78663865
  44       -0.83079609    -4.46537301    -3.01797346
  45       -3.49031104    -2.62275144    -3.92357919
END

 SPECIES   NONLINRP

 ELEC
  6   0.0
 END
*START

 INITGEO  GEOM
```

STATUS 2

GEOM

1	5.24654048	6.53777611	2.52533516
2	4.70236084	5.77595094	0.04807728
3	2.33136374	4.83584617	-0.53956582
4	0.45169610	4.63441805	1.36596988
5	1.03476192	5.43471624	3.86153895
6	3.41431617	6.36846565	4.43219800
7	-1.96548573	3.58194202	0.90191789
8	-2.70702934	2.25816918	-1.27789275
9	-5.46852505	1.82907206	-1.72735133
10	-6.83487912	0.06301112	-0.27102089
11	-9.41131980	-0.28400265	-0.80368124
12	-10.61413660	1.09913651	-2.69804826
13	-9.24643967	2.84772203	-4.12470806
14	-6.67534675	3.19226912	-3.64007461
15	-5.55116751	-1.44429133	1.71377176
16	-6.89205090	-2.36791681	3.80630017
17	-5.69732192	-3.78747312	5.68124850
18	-3.11366865	-4.28622146	5.50978667
19	-1.73855966	-3.34697563	3.46261196
20	-2.93294542	-1.94196180	1.57299548
21	-1.35638082	-1.03343637	-0.62790207
22	-1.86857912	-2.34843072	-3.14187005
23	1.06707420	-0.73990068	-0.08883052
24	4.27195778	-1.83030988	-1.03026706
25	4.15397784	-6.05110455	-1.06113933
26	6.97302786	-0.44846794	1.89688558
27	5.21905755	-0.28305920	-4.86183855
28	-8.88652975	-1.93760702	3.99723540
29	0.27184073	-3.70597722	3.31333064
30	-2.16549753	-5.38002587	6.96249008
31	-6.78266858	-4.47784776	7.27877750
32	-10.47775040	-1.69118486	0.23632696
33	-5.59141440	4.53574868	-4.74991767
34	-12.60587870	0.78767478	-3.07530983
35	-10.16264110	3.92215182	-5.61188552
36	-3.28415132	3.60311421	2.48044727
37	1.92535420	4.25577227	-2.45859715
38	-0.39895600	5.27596326	5.31979639
39	6.14047539	5.90379625	-1.40503113
40	3.86174405	6.95764880	6.34323211
41	7.11085279	7.26524922	2.97399159
42	-1.62556099	2.64608006	-2.98042902
43	-0.79230941	-1.45174863	-4.65701336

```
 44       -1.19737011     -4.29470884     -2.92133099
 45       -3.86856010     -2.38897846     -3.62329662
END

 SPECIES   NONLINTS

 ELEC
  6   0.0
 END

*PATH

 SCALEMASS 1.00
 FREQSCALE 0.964
 SSTEP     0.01
 INH       9
 INTMU     3
 RPM       pagem
 RODS  ON

 COORD  CURV3
 INTDEF
 2-1 3-2 4-3 5-4 6-5 7-4 8-7 9-8 10-9 11-10
 12-11 13-12 14-13 15-10 16-15 17-16 18-17
 19-18 20-19 21-20 22-21 23-21 24-23 25-24
 26-24 27-24 28-16 29-19 30-18 31-17 32-11
 33-14 34-12 35-13 36-7 37-3 38-5 39-2 40-6
 41-1 42-8 43-22 44-22 45-22
 3-2-1 4-3-2 5-4-3 6-5-4 7-4-3 8-7-4 9-8-7
 10-9-8 11-10-9 12-11-10 13-12-11 14-13-12
 15-10-9 16-15-10 17-16-15 18-17-16 19-18-17
 20-19-18 21-20-15 22-21-20 23-21-20 24-23-21
 25-24-23 26-24-23 27-24-23 28-16-15 29-19-20
 30-18-19 31-17-16 32-11-10 33-14-9 34-12-11
 35-13-14 36-7-8 37-3-4 38-5-4 39-2-3 40-6-5
 41-1-2 42-8-9 43-22-21 44-22-21 45-22-21
 4-3-2-1 5-4-3-2 6-5-4-3 7-4-3-2 8-7-4-3
 9-8-7-4 10-9-8-7 11-10-9-8 12-11-10-9
 13-12-11-10 14-13-12-11 15-10-9-14
 16-15-10-9 17-16-15-10 18-17-16-15
 19-18-17-16 20-19-18-17 21-20-15-16
 22-21-20-15 23-21-20-15 24-23-21-20
 25-24-23-21 26-24-23-21 27-24-23-21
 28-16-15-20 29-19-20-15 30-18-19-20
 31-17-16-15 32-11-10-15 33-14-9-10
 34-12-11-10 35-13-14-9 36-7-8-9
```

```
 37-3-4-7 38-5-4-7 39-2-3-4 40-6-5-4
 41-1-2-3 42-8-9-10 43-22-21-20 44-22-21-20
 45-22-21-20
 END

 SRANGE
   SLP       1.5
   SLM       -1.5
  END

 SPECSTOP
  CURVE vag
  POINT savegrid
  PERCENTDOWN 95.0
 END

 PRPATH
 COORD 8 21
 INTERVAL  1
 xmol
 END
*TUNNEL
 QUAD
   NQE 40
   NQTH 40
 END

   SCT

*RATE

 FORWARDK
 SIGMAF   1
 CVT
 PRDELG ON

 TEMP
 293.
 298.
 303.
 END
```

Job.70

```
*GRGENERAL

 GRRESTART
```

```
 RSTTOL 1E-4

*GRCOMMON

 GRENER
  #p b3lyp/6-31+g* empiricaldispersion=gd3bj scf=tight
  scrf=(cpcm,solvent=dichloroethane) UNITS=AU FCHK NOSYMM integral(ultrafine)
 END

 GRFIRST
  #p b3lyp/6-31+g* FORCE empiricaldispersion=gd3bj scf=tight
  scrf=(cpcm,solvent=dichloroethane) UNITS=AU FCHK NOSYMM integral(ultrafine)
 END

 GRSEC
  #p b3lyp/6-31+g* FREQ=NORAMAN empiricaldispersion=gd3bj
  scrf=(cpcm,solvent=dichloroethane) UNITS=AU FCHK NOSYMM integral(ultrafine)
  scf=tight
 END

 GRLINK0
  %mem=6GB
  %nprocs=32
  %chk=g09.chk
 END

*GRREACT1

 CHARGE        0
 MULTIPLICITY   6

*GRPROD1

 CHARGE        0
 MULTIPLICITY   6

*GRSTART

 CHARGE        0
 MULTIPLICITY   6
*GRPATH

 GRENER
  #p b3lyp/6-31+g* guess=tcheck empiricaldispersion=gd3bj
  scrf=(cpcm,solvent=dichloroethane) UNITS=AU FCHK NOSYMM
  integral(ultrafine) scf=tight
```

```
END

GRFIRST
 #p b3lyp/6-31+g* FORCE guess=tcheck empiricaldispersion=gd3bj
 scrf=(cpcm,solvent=dichloroethane) UNITS=AU FCHK NOSYMM
 integral(ultrafine) scf=tight
END

GRSEC
 #p b3lyp/6-31+g* FREQ=NORAMAN guess=tcheck empiricaldispersion=gd3bj
 scrf=(cpcm,solvent=dichloroethane) UNITS=AU FCHK NOSYMM
 integral(ultrafine) scf=tight
END
```

Supplementary References

1. McAtee, C. C.; Riehl, P. S.; Schindler, C. S. Polycyclic Aromatic Hydrocarbons via Iron(III)-Catalyzed Carbonyl–Olefin Metathesis. *J. Am. Chem. Soc.* **2017**, *139*, 2960–2963.
2. Bannwarth, C.; Caldeweyher, E.; Ehlert, S.; Hansen, A.; Pracht, P.; Seibert, J.; Spicher, S.; Grimme, S. Extended tight-binding quantum chemistry methods. *WIREs Comput. Mol. Sci.* **2021**, *11*, e1493.
3. Becke, A. D., Density-functional thermochemistry. III. The role of exact exchange. *J. Chem. Phys*. **1993**, *98*, 5648 - 5652.
4. Hehre, W. J.; Stewart, R. F.; Pople, J. A., Self-Consistent Molecular-Orbital Methods. I. Use of Gaussian Expansions of Slater-Type Atomic Orbitals. *J. Chem. Phys* **1969**, *51*, 2657 - 2664.
5. Miertus, S.; Scrocco, E.; Tomasi, J., Electrostatic Interaction of a Solute with a Continuum - a Direct Utilization of Ab initio Molecular Potentials for the Prevision of Solvent Effects. *Chem. Phys*. **1981**, 55, 117 - 129.
6. Frisch, M. J.; Trucks, G. W.; Schlegel, H. B.; Scuseria, G. E.; Robb, M. A.; Cheeseman, J. R.; Scalmani, G.; Barone, V.; Petersson, G. A.; Nakatsuji, H.; Li, X.; Caricato, M.; Marenich, A. V.; Bloino, J.; Janesko, B. G.; Gomperts, R.; Mennucci, B.; Hratchian, H. P.; Ortiz, J. V.; Izmaylov, A. F.; Sonnenberg, J. L.; Williams-Young, D.; Ding, F.; Lipparini, F.; Egidi, F.; Goings, J.; Peng, B.; Petrone, A.; Henderson, T.; Ranasinghe, D.; Zakrzewski, V. G.; Gao, J.; Rega, N.; Zheng, G.; Liang, W.; Hada, M.; Ehara, M.; Toyota,

K.; Fukuda, R.; Hasegawa, J.; Ishida, M.; Nakajima, T.; Honda, Y.; Kitao, O.; Nakai, H.; Vreven, T.; Throssell, K.; Montgomery Jr., J. A.; Peralta, J. E.; Ogliaro, F.; Bearpark, M. J.; Heyd, J. J.; Brothers, E. N.; Kudin, K. N.; Staroverov, V. N.; Keith, T. A.; Kobayashi, R.; Normand, J.; Raghavachari, K.; Rendell, A. P.; Burant, J. C.; Iyengar, S. S.; Tomasi, J.; Cossi, M.; Millam, J. M.; Klene, M.; Adamo, C.; Cammi, R.; Ochterski, J. W.; Martin, R. L.; Morokuma, K.; Farkas, O.; Foresman, J. B.; Fox, D. J. Gaussian 16 Rev. C.01, Wallingford, CT, **2016**.

7. Perdew, J. P.; Burke, K.; Ernzerhof, M. Generalized Gradient Approximation Made Simple. *Phys. Rev. Lett.* **1996**, *77*, 3865–3868.
8. Bigeleisen, J.; Mayer, M. G. *J. Chem. Phys.* **1947**, *15*, 261.
9. Anderson, T. L.; Kwan, E. E. *PyQuiver* **2020**, www.github.com/ekwan/PyQuiver
10. Saunders, M.; Laidig, K. E.; Wolfsberg, M. Theoretical Calculation of Equilibrium Isotope Effects Using Ab Initio Force Constants: Application to NMR Isotope Perturbation Studies. *J. Am. Chem. Soc.* **1989**, *111*, 8989–8994.
11. Weigend, F; Ahlrichs, R; Balanced basis sets of split valences, triple zeta valence and quadruple zeta valence quality for H to Rn: Design and assessment of accuracy *Phys. Chem. Chem. Phys.*, 2005,**7**, 3297-3305
12. VandeVondele, J.; Krack, M.; Mohamed, F.; Parrinello, M.; Chassaing, T.; Hutter, J. Quickstep: Fast and Accurate Density Functional Calculations Using a Mixed Gaussian and Plane Waves Approach. *Comput. Phys. Commun.* **2005**, *167*, 103–128.
13. Goedecker, S.; Teter, M.; Hutter, J. Separable Dual-Space Gaussian Pseudopotentials. *Phys. Rev. B* **1996**, *54*, 1703–1710.
14. Zheng, J.; Bao, J. L.; Meana-Pañeda, R.; Zhang, S.; Lynch, B. J.; Corchado, J. C.; Chuang, Y.-Y.; Fast, P. L.; Hu, W.-P.; Liu, Y.-P.; Lynch, G. C.; Nguyen, K. A.; Jackels, C. F.; Fernandez Ramos, A.;Ellingson, B. A.; Melissas, V. S.; Villà, J. Rossi, I.; Coitiño, E. L.; Pu, J.; Albu, T. V.; Ratkiewicz, A.; Steckler, R.; Garrett, B. C.; Isaacson, A. D.; Truhlar, D. G. *Polyrate*-version 2017-C; University of Minnesota: Minneapolis, 2017.
15. Singleton, D. A.; Hang, C.; Szymanski, M. J.; Greenwald, E. E. A New Form of Kinetic Isotope Effect. Dynamic Effects on Isotopic Selectivity and Regioselectivity. *J. Am. Chem. Soc.* **2003**, 125, 1176– 1177, DOI: 10.1021/ja027221k

16. Schindler, C.; Kwan, E.; Vonesh, H.; Wagen, C.; McMinn, S.; Thedford, J. Inadequacy of Continuum Solvation for Polar Reactions: Predicting the Mechanism of Carbonyl–Olefin Metathesis. *ChemRxiv* **2022**, DOI: 10.26434/chemrxiv-2022-nnp81.

